Response to Reviewer #1

Reviewer # 1 Review:

The manuscript entitled, "New Insights into Atmospherically Relevant Reaction Systems using Direct Analysis in Real Time Mass Spectrometry (DART-MS)", by Zhao et al., describes a series of measurements examining the uptake of amines onto diacid aerosols and chemical composition measurements of cedrene SOA. The detection of amine reactions or composition by DART-MS enabled the authors to quantify, quite elegantly, differences between odd and even numbered diacids. The differences between these diacids are quite dramatic and the authors have done an excellent job of quantifying this and explaining the mechanism. The manuscript is well written and the data robust with good quantitative analysis. The authors have done an extensive job in evaluating potential artifacts in DART and interferences as reported in the main text and supplementary information. I recommend publication of the manuscript.

Response: We thank the reviewer for the positive evaluation of the manuscript.

Response to Reviewer #2

We thank the reviewer for the helpful comments on the manuscript. Our point-to-point responses to each comment are as follows *(reviewer comments are in black, and author responses are in blue).*

This is a well written manuscript reporting on the application of DART-MS for in-situ analysis aerosolized particles of C_3-C_7 dicarboxylic acids reacted with gas-phase amines and laboratory SOA generated by ozonolysis of alpha-cedrene – all are model systems relevant to atmospheric aerosols. The results show that DART–MS has a good potential for molecular-level analysis of aerosol mixtures with enhanced sensitivity to shallow surface (~30 nm) layer of particles. Complemented by more traditional AMS detection of the whole particle volumes, DART-MS can provide unique information on the surface chemistry of particles. The presented results are thoroughly evaluated in a context of available literature reports and are convincing. Overall, this is an accomplished work in all its aspects including scientific impact, original measurements, methodology development, and presentation quality. I recommend this paper for publication. Below, I list a few minor notes to consider in the revised manuscript.

Response: We thank the reviewer for the positive evaluation of the manuscript.

I think that quantitative estimate of the surface layer (~30 nm) probed by DART is a very important result that needs to be included in the abstract.

Response: We have included a sentence "Results show that DART-MS probes ~ 30 nm of the surface layer" in the abstract.

Line 24: 'particles' after (SOA) can be removed

Response: We have removed it.

Line 33: 'However' is not needed.

Response: We have removed it.

Eq (1): it needs to be noted that eq 1 assumes the same effective ionization efficiency for gas-phase and particle phase amines that likely won't be always correct.

Response: We have added a sentence "assuming the same ionization efficiency for the gas-phase and particle-phase amines" before the sentence "the fraction of amine taken up by the particles (f_p) can be derived from Eq. (1)".

Line 205, eq 2, and then throughout the text: it is more common to use 'normalized surface area' rather than 'surface area normalized'.

Response: In this paper, the particle-phase fraction of amines is normalized to the surface area of the particles. We think the expression "surface area normalized …" is more appropriate than "normalized surface area …".

For clarity we have modified the sentence on lines 206-207 to read "Thus, the particle-phase fraction of amine taken up by the diacid, normalized by surface area, (F_p) is given by:…"

Line 293: consider change of 'explanation is the relative: : :" to something like 'a possible explanation can be suggested based on differences in the relative saturation vapor pressures'

Response: We have changed "a possible explanation is…" to "a possible explanation can be suggested based on differences in…".

We have also made some minor editorial changes for clarification in several places in the manuscript:

Page 7 line 145-146: The following was added "The SMPS was operated with a sheath flow of 3 LPM and an aerosol flow of 0.3 LPM."

Page 7 lines 170-171: Details of the sheath and aerosol flows were added so that it reads "Size distributions of SOA particles formed in the flow reactor at the two residence times (44 or 27 s) were also measured using SMPS (sheath and aerosol flows were 15 LPM and 1.5 LPM, respectively).

Page 7 lines 171-173: For clarification, the sentence was changed to read: "Typical surface weighted geometric mean diameters ($\overline{D}_{g,S}$) were measured to be 28 nm and 21 nm, and number weighted diameters were ($\overline{D}_{g,N}$) of 24 and 16 nm, respectively."

Page 8 line 185: "is" was replaced with "was" so that it reads "The DART probe was placed at the entrance of the MS…"

Page 12 lines 303-305: "data" was changed to "value" and "suggest" was changed to "suggests" so that it reads "the F_p value (Fig. 2) for the BA reaction suggests that…"

Page 13 lines 328-330: The unit of "g cm^{-3}" was removed from line 328 and was added to each density value so that it reads "amine-reacted diacid particles, which is assumed to be the same as the solid diacid samples (i.e., 1.619 g cm^{-3} for malonic acid, 1.429 g cm^{-3} for glutaric acid, and 1.329 g cm^{-3} for pimelic acid..."

Figure 2 caption: "fraction" was added so that it reads "Surface area normalized fraction…"

Figure 3 caption: "Surface area normalized fraction" replaced "Particle phase fraction" so that it reads "Surface area normalized fraction, F_p, of…"

We have also made some minor editorial changes for clarification in the Supporting Information:

Page 2 line 41: "F_p" has been replaced with "f_p"

Figure S2a: Reformatted the y-axis.

Page 6 line 78: "and" was replaced with "or" so that it reads "particle stream or standard solutions"

Page 6 line 78 added after "standard solutions," "but the ammonium adduct of the diacid was observed due to the ubiquitous presence of NH_3 in room air."

Figure S4: Peak labelling was reformatted and the ammonium adduct label was added to Fig. S4a.

New insights into atmospherically relevant reaction systems using direct analysis in real time-mass spectrometry (DART-MS)

Yue Zhao, Michelle C. Fairhurst, Lisa M. Wingen, Véronique Perraud, Michael J. Ezell, and Barbara J. Finlayson-Pitts*

Department of Chemistry
University of California
Irvine, CA 92697, USA

Revision for
Atmospheric Measurement Techniques
February 21, 2017

*Corresponding author: Email: bjfinlay@uci.edu; phone: (949) 824-7670; Fax: (949) 824-2420

Abstract

The application of direct analysis in real time mass spectrometry (DART-MS), which is finding increasing use in atmospheric chemistry, to two different laboratory model systems for airborne particles is investigated: (1) submicron C_3-C_7 dicarboxylic acid (diacid) particles reacted with gas phase trimethylamine (TMA) or butylamine (BA); (2) secondary organic aerosol (SOA) particles from the ozonolysis of α-cedrene. The diacid particles exhibit a clear odd-even pattern in their chemical reactivity toward TMA and BA, with the odd-carbon diacid particles being substantially more reactive than even ones. The ratio of base to acids in reacted particles, determined using known acid-base mixtures, was compared to that measured by high resolution time-of-flight aerosol mass spectrometry (HR-ToF-AMS), which vaporizes the whole particle. Results show that DART-MS probes ~30 nm of the surface layer, consistent with other studies on different systems. For α-cedrene SOA particles, it is shown that varying the temperature of the particle stream as it enters the DART-MS ionization region can distinguish between specific components with the same molecular mass but different vapor pressures. These results demonstrate the utility of DART-MS for (1) examining reactivity of heterogeneous model systems for atmospheric particles and (2) probing components of SOA particles based on volatility.

1. Introduction

Organic aerosol (OA) particles are responsible for ~ 20-90% of atmospheric submicron particulate matter, with a substantial fraction being secondary organic aerosol (SOA) formed via oxidation of volatile organic compounds (VOCs) (Zhang et al., 2007;Jimenez et al., 2009;Hallquist et al., 2009;Ng et al., 2010;Finlayson-Pitts and Pitts, 2000). As a result, the chemistry and physics of OA particles have been of great interest to the atmospheric science community over decades. Despite significant progress, many physicochemical processes of OA particles such as formation, growth, aging, and water uptake remain to be quantitatively understood which is essential for a better understanding of their impacts on air quality, human health, visibility and climate (Kroll and Seinfeld, 2008;Hallquist et al., 2009;Laskin et al., 2015;Ziemann and Atkinson, 2012;Noziere et al., 2015;Glasius and Goldstein, 2016;George et al., 2015;Moise et al., 2015;Farmer et al., 2015). Atmospheric OA particles consist of hundreds to thousands of organic compounds with a wide range of functionality, solubility, polarity, and volatility, and hence pose many challenges and difficulties for characterization of their molecular composition (Hallquist et al., 2009;Noziere et al., 2015;Glasius and Goldstein, 2016). Therefore, there is a critical need for implementation of analytical instrumentation which can be applied to elucidating the composition of OA particles.

Recent advances in the development and application of mass spectrometry (MS) techniques for the analysis of OA particles have been documented in a number of reviews (Noziere et al., 2015;Laskin et al., 2012;Laskin et al., 2013;Nizkorodov et al., 2011;Pratt and Prather, 2012a, b). Online particle MS techniques that use relatively high energy vaporization and ionization processes, e.g., flash vaporization of particles followed by electron ionization (EI) (DeCarlo et al., 2006;Tobias et al., 2000;Smith et al., 2004) or laser ablation and ionization (Gard et al., 1997;Zelenyuk and Imre, 2005;Murphy and Thomson, 1995), have advantages of high time resolution and real-time quantitative information on composition (DeCarlo et al., 2006;Zhang et al., 2007;Jimenez et al., 2009;Ng et al., 2010;Murphy and Thomson, 1995;Tobias et al., 2000;Zelenyuk and Imre, 2005;Gard et al., 1997;Pratt and Prather, 2012a, b). However, these techniques typically cause extensive fragmentation of molecules, providing elemental information but limited molecular information on individual organic components.

In contrast, a number of soft-ionization techniques such as electrospray ionization (ESI),

Comment [b1]: deleted "particles"

Comment [b2]: "However" omitted

chemical ionization, and photoionization have been deployed to probe the molecular composition of atmospheric OA particles (Laskin et al., 2012;Laskin et al., 2013;Nizkorodov et al., 2011;Pratt and Prather, 2012a, b). Variants of ESI such as extractive electrospray ionization mass spectrometry (EESI-MS) (Chen et al., 2006), have recently been applied to the real-time measurement of the molecular composition of OA particles (Doezema et al., 2012;Gallimore and Kalberer, 2013;Horan et al., 2012). In this technique, analyte ionization occurs when the charged solvent spray intersects the sample stream in front of the MS inlet. However, the mechanism for the interaction between charged solvent droplets and samples is not yet well understood (Law et al., 2010;Gallimore and Kalberer, 2013;Jackson et al., 2008;Chen et al., 2006;Chingin et al., 2008;Wang et al., 2012;Chen et al., 2007). In addition, the use of charged solvent sprays may lead to in-source ion clustering of analytes, which is prone to occur in ESI-MS (Gao et al., 2010;Muller et al., 2009b). Chemical ionization mass spectrometry (CIMS) has the advantages of high sensitivity and selectivity, high time resolution, and has been applied to online detection of a variety of inorganic and organic gases (Huey, 2007;Noziere et al., 2015). Recently, CIMS employing thermal desorption techniques has been used to measure the molecular composition of OA particles collected onto a substrate (Smith et al., 2004;Winkler et al., 2012;Bzdek et al., 2014;Yatavelli et al., 2012;Lopez-Hilfiker et al., 2014;Aljawhary et al., 2013). As the CIMS technique with a specific reagent ion is highly selective toward certain classes of organic compounds, a comprehensive analysis of the molecular composition of OA particles may require the use of multiple reagent ions. In addition, CIMS is also possibly subject to artifacts from gas phase ion-clustering (Aljawhary et al., 2013).

Direct analysis in real-time mass spectrometry (DART-MS) is an atmospheric pressure soft ionization technique allowing for real-time *in situ* characterization of the molecular composition of gaseous, liquid, and solid samples with a wide range of polarities (Cody et al., 2005;Gross, 2014). The samples are directly introduced into the ionization region between the DART ion source and the MS inlet, where a heated helium gas flow containing metastable helium atoms (He*) generated by a corona discharge is used to thermally volatilize and ionize the sample. Under ambient laboratory conditions, ionization of the analyte occurs primarily through a series of reactions with secondary species such as protonated water clusters, molecular oxygen ions (O_2^+), and superoxide anions (O_2^-), generated by the reactions between He* species and atmospheric water and oxygen molecules. The result is the production of mainly $[M+H]^+$, M^+,

and $[M-H]^+$ ions in the positive ion mode, and $[M-H]^-$ and M^- ions in the negative ion mode (Cody et al., 2005;Nah et al., 2013;Gross, 2014).

DART-MS has been widely applied to explosive detection, forensic analysis, food analysis, and clinical and pharmaceutical studies (see the review by Gross (2014) and references therein) as well as to the analysis of OA particles (Chan et al., 2013;Nah et al., 2013;Chan et al., 2014;Davies and Wilson, 2015;Zhou et al., 2015;Schilling Fahnestock et al., 2015;Zhao et al., 2016). For example, Wilson and coworkers demonstrated that DART-MS probes several nanometers of the surface layer (Nah et al., 2013;Chan et al., 2013) and applied this technique to investigate the bulk and interface regions of particles during reaction (Nah et al., 2013;Chan et al., 2013;Chan et al., 2014;Davies and Wilson, 2015). Zhou et al. (Zhou et al., 2015) employed DART-MS to study the heterogeneous reactions of O_3 with polycyclic aromatic hydrocarbon films coated on the tip of a glass melting point capillary tube. Schilling Fahnestock et al. (Schilling Fahnestock et al., 2015) recently reported the first application of DART-MS for off-line analysis of the composition of SOA from photooxidation of C_{12} alkanes. In a limited comparison of DART-MS to ESI-MS, Zhao et al. (Zhao et al., 2016) reported that spectra of particles from α-cedrene ozonolysis were similar using the two techniques.

In this study, we explore the online application of DART-MS to particles from the reaction of submicron dicarboxylic acid (diacid) particles with gas phase trimethylamine (TMA) or butylamine (BA) and also report more detailed studies on SOA particles from ozonolysis of the sesquiterpene α-cedrene ($C_{15}H_{24}$). For comparison, measurements by high resolution time-of-flight aerosol mass spectrometry (HR-ToF-AMS) were also carried out on selected amine-acid reacted particles. Diacids are among the most abundant components of atmospheric particles, with a dominant source from photochemical and aqueous phase oxidation processes (Kawamura and Bikkina, 2016;Ervens et al., 2011;Herrmann et al., 2015). Amines, which are ubiquitous in air (Ge et al., 2011), play an important role in particle nucleation and growth (Zhang et al., 2012;Kulmala et al., 2014;Dawson et al., 2012;Chen et al., 2016), formation of light-absorbing OA particles (Laskin et al., 2015;De Haan et al., 2011;Powelson et al., 2014;Duporte et al., 2016), as well as aging of OA particles (Laskin et al., 2015;Muller et al., 2009a). Results from this study provide additional support for the application of DART-MS to probe heterogeneous atmospheric reactions, and to provide additional insights into the nature of organic constituents in complex SOA particles.

2. Experimental

2.1 Generation and reaction of diacid particles with gas phase amines

Figure 1 is a schematic diagram of the glass flow reactor (Zhao et al., 2015) used to investigate reactions between gas phase amines (trimethylamine or butylamine) and particles of malonic acid (C_3), succinic acid (C_4), glutaric acid (C_5), adipic acid (C_6), and pimelic acid (C_7). Gas phase trimethylamine (TMA) was generated by passing 1.0 L min^{-1} of clean dry air (Praxair, ultra zero air) through a U-shaped glass holder containing pure liquid TMA sealed inside a permeation tube (VICI Metronics Inc). Generation of gas phase butylamine (BA) was achieved by injecting an aqueous solution (1% v/v), prepared from pure liquid BA (Sigma-Aldrich, 99.5%) and nanopure water (18.2 MΩ cm), into a flow of 0.5 L min^{-1} of dry air using an automated syringe pump (Pump Systems Inc., model NE-1000) at a rate of 2.4 μL hr^{-1}. The concentration of TMA in the air flow exiting the permeation tube was measured by collection onto a weak cation exchange resin followed by extraction and analysis using ion chromatography as described previously (Dawson et al., 2014). The initial concentration of TMA in the flow reactor was calculated to be 50 ppb based on the measured concentration from the permeation tube and the dilution factor. The initial concentration of BA, calculated from the amount of the aqueous solution injected and the total air flow in the reactor, was also 50 ppb.

For each experiment, the flow reactor was first conditioned overnight with either 1.0 L min^{-1} TMA or 0.5 L min^{-1} BA in addition to clean, dry air so that the total flow was ~ 2 L min^{-1}. When the gas phase concentration of the amine became stable as indicated by DART-MS signals, a small flow (0.2-0.5 L min^{-1}) of air containing dry diacid particles was added to the flow reactor upstream of the amine inlet. The flow of clean, dry air was adjusted to bring the total flow in the reactor to 2.0 L min^{-1} corresponding to a residence time of 44 s. Acid particles were generated by atomizing aqueous solutions of the corresponding diacid (1 g L^{-1} in nanopure water) using an atomizer (TSI, model 3076) and dried by passing through two diffusion dryers in series (TSI, model 3062). The desiccant inside the dryers was replaced daily to minimize water associated with the particles. The relative humidity (RH) in the flow reactor was < 5% as measured by a humidity probe (Vaisala, HMT234). All diacids were purchased from Sigma-Aldrich and have a stated purity of > 99 %. The size distribution of the particles formed in the flow reactor was measured using a scanning mobility particle sizer (SMPS, TSI) consisting of an electrostatic

classifier (model 3080), a long differential mobility analyzer (model 3081), and a condensation particle counter (model 3025A or 3776). The SMPS was operated with a sheath flow of 3 LPM and an aerosol flow of 0.3 LPM. Because the flow system required extensive conditioning with the amine prior to introducing the diacid particles, the size distributions represent particles after reaction with amines. Typical surface weighted size distributions are shown in Fig. S1, and the different weighted geometric mean diameters ($\bar{D}_{g,x}$, where x = number (N), surface (S), or volume (V)) and the total concentrations for all diacid particles are given in Table S1.

The amine-reacted particle stream (PS) exiting the flow reactor was either directly introduced into the DART ionization region for online measurement of the total (gas phase + particle-bound) amines, or passed through a 10 cm monolith carbon denuder (Novacarb^{TM}; Mast Carbon, Ltd.) to remove gases and measure only particle-bound amines and diacids. The denuder was maintained at room temperature (T_{PS} = 23 ^{o}C). As discussed below, the fraction of particle-bound amines was corrected for particle loss in the denuder, which was ~ 10 % at room temperature (Fig. S1).

2.2 α-Cedrene SOA particles generation

Ozonolysis of α-cedrene in the absence of seed particles or OH scavengers was used to generate SOA particles under dry conditions in the glass flow reactor described previously (Zhao et al., 2016). Gas phase α-cedrene was generated by injecting the pure liquid (Sigma-Aldrich, > 98%) into a flow (1.8 or 3.0 L min^{-1}) of clean, dry air using an automated syringe pump. Ozone, produced by passing a flow of 0.24 L min^{-1} of O_2 (Praxair, Ultra High Purity, 99.993%) through a Pen-Ray mercury lamp (model 11SC-2) was added to the flow reactor downstream of the α-cedrene inlet. The total gas flow in the reactor was 2.0 or 3.2 L min^{-1}, giving a residence time of 44 or 27 s, respectively. The initial α-cedrene concentration, calculated from the amount of α-cedrene liquid injected into the reactor and the total gas flow, was 138 ppb. The initial O_3 concentration, measured at the source using a UV-VIS spectrometer (Ocean Optics, HR4000), was calculated to be 16 ppm in the reactor after dilution.

Size distributions of SOA particles formed in the flow reactor at the two residence times (44 or 27 s) were also measured using SMPS (sheath and aerosol flows were 15 LPM and 1.5 LPM, respectively). Typical surface weighted geometric mean diameters ($\bar{D}_{g,S}$) were measured to be 28 nm and 21 nm, and number weighted diameters were ($\bar{D}_{g,N}$) of 24 and 16 nm, respectively. Once

Comment [b3]: added

Comment [b4]: added for clarity

Comment [b5]: reworded for clarity

stable, the chemical composition of these particles at both reaction times was measured online using DART-MS. Before entering into the DART ionization region, 2.0 L min^{-1} of particle stream (PS) exiting the reactor was first passed through a 10 cm monolith carbon denuder to remove the gas phase species and then heated to different temperatures (up to T_{PS} =160 ^{o}C) in a stainless steel tube wrapped with a heating tape. The residence time of the particle stream in the heated tube was ~ 4 s. Although the use of the denuder caused a ~ 30% loss of SOA particles at room temperature, it has no significant influence on the size distribution for which a typical example is shown in Fig. S2.

2.3 DART-MS measurements operating conditions

The chemical composition of either amine-reacted diacid particles or α-cedrene SOA particles was measured online using a Xevo TQS triple quadrupole mass spectrometer (Waters) equipped with a commercial DART ion source (IonSense, DART SVP with Vapur® Interface). The DART probe was placed at the entrance of the MS, with a distance of 5 mm and a relative angle of 180^{o} (Fig. 1), and was operated under the following conditions: He reagent gas flow 3.1 L min^{-1}; He gas temperature 350 ^{o}C (which gives a measured temperature of ~ 260 ^{o}C in the ionization region with or without particle stream flow (Fig. S3)); grid electrode voltage 350 V. Mass spectra were collected in the range *m/z* 20-500 for the amine-diacid particle system and *m/z* 100-1000 for α-cedrene SOA particles. Each spectrum was acquired by averaging the signal over 2-4 min of sampling time. Background spectra were also recorded by measuring a clean air stream under conditions identical to those for online particle stream measurements and subtracted from particle spectra.

2.4 DART-MS analysis of amine-reacted diacid particles

For the amine-diacid particle system, both the gas phase and particle-bound amines were detected as $[M+H]^+$ ions in the positive ion mode, and the diacids as $[M-H]^-$ in the negative ion mode. Diacid-amine clusters were not observed in the mass spectra (Fig. S4). As described earlier, the particle-bound and the total (gas phase + particle-bound) amines can be measured in the presence and absence of a denuder, respectively. Thus, assuming the same ionization efficiency for the gas-phase and particle-phase amines, the fraction of amine taken up by the particles (f_p) can be derived from Eq. (1),

Comment [b6]: changed "is" to "eas"

Comment [b7]: sentence added

$$f_p = \frac{amine\ ion\ signal\ measured\ with\ denuder \times C_f}{amine\ ion\ signal\ measured\ without\ denuder} \quad (1)$$

where C_f is the correction factor for the particle loss in the denuder and has a value of 1.1 (SI section 1). The value of f_p can be an indicator of the reactivity of diacid particles toward amines. Given the difference in surface area concentrations of different diacid particles (Table S1), the measured f_p was normalized to an arbitrary reference surface area of 1×10^{-4} cm^2 cm^{-3} for direct comparisons of the reactivity of different amine-diacid systems. Thus, the particle-phase fraction of amine taken up by the diacid normalized by surface area, (F_p) is given by:

Comment [b8]: reworded for clarity

$$F_p = \frac{f_p}{\frac{aerosol\ surface\ area\ concentration\ (cm^2\ cm^{-3})}{reference\ surface\ area\ (cm^2\ cm^{-3})}} \quad (2)$$

The molar ratio ($R_{B/A}$) of amine (base, B) to diacid (A) in amine-reacted diacid particles can also provide important insights into the reactivity of the diacid particles toward amines. Values of $R_{B/A}$ were derived first from four aqueous standard solutions with different amine concentrations (0.5-10 mM) but constant diacid concentrations (10 mM) for each amine-diacid system. As shown below, this covers the range measured for the reacted particles. A melting point capillary tube was dipped into the standard solution and immediately placed into the DART ionization region for analysis. A linear relationship between the base-to-acid molar ratio ($R_{B/A}$) of the aqueous solutions and the corresponding DART-MS signal ratios for amine ($[M+H]^+$) to acid ($[M-H]^-$) was observed for each standard solution (Fig. S5). These relationships were then used to estimate the $R_{B/A}$ value in amine-reacted diacid particles.

2.5 DART-MS analysis of α-cedrene SOA particles

α-Cedrene SOA particles were analyzed in the negative ion mode, where the deprotonated $[M-H]^-$ ions dominate. In other studies, DART-MS was proposed to preferentially probe the surface layers of particles and the measured ion signal was sensitive to the volatility of the analytes (Nah et al., 2013;Chan et al., 2013). In the present studies, the gas phase species were removed by a denuder and the particle stream was then exposed to temperatures up to 160 ^oC prior to introduction into the DART ionization region in order to probe the bulk of the particles and low volatility components of SOA particles such as HMW products.

2.6 HR-TOF-AMS measurements

In some experiments, the chemical composition of TMA-reacted diacid particles was also analyzed online using an Aerodyne high resolution aerosol mass spectrometer (HR-ToF-AMS). Analysis of HR-ToF-AMS high resolution mass spectra was carried out using SQUIRREL V1.56D-1.57I and PIKA V1.15D-1.61I analysis software with IGOR Pro (Wavemetrics, Inc.). Default values for the fragmentation tables were used except for corrections to the isotopic abundance of $^{15}N^{14}N$ which is not resolved from CHO^+ at *m/z* 29 and was quantified for each experiment with the use of a particle filter (Canagaratna et al., 2015). Default relative ionization efficiencies (RIE) values were used for all organics, while that for TMA was measured as discussed in the SI (section 5). TMA-reacted diacid particles with and without a denuder gave similar results and were averaged to generate mass spectra for each TMA-diacid system (Fig. S6). From these mass spectra, the ratio of $C_xH_yN_1^+$ fragments to the sum of $C_xH_y^+$ and $C_xH_yO_z^+$ fragments, which is a measure of the ratio of amine to diacid, was determined for each TMA-diacid system (Fig. S7). Because these particles are efficiently vaporized at the vaporizer temperature employed (T_{vap} = 600°), the amine to diacid ratios from HR-ToF-AMS measurements reflect the overall composition of the particle ensemble.

3. Results and Discussion

3.1 Reaction of diacid particles with gas phase amines

3.1.1 DART-MS data

Figure 2 shows the surface area normalized fraction (F_p) of BA or TMA in the particle phase of amine-reacted C_3-C_7 diacid particles as a function of carbon number. The odd-carbon diacids take up much more base than the even-carbon acids, with no particle-bound amines detected for the C_4 and C_6 acids. The measured F_p values for both amines decrease with increasing carbon number, with no particle bound TMA observed for pimelic acid (C_7). An odd-even alternation in physical properties such as melting point (Thalladi et al., 2000), vapor pressure (Bilde et al., 2003;Bilde et al., 2015;Cappa et al., 2007;Bruns et al., 2012), and solubility (Zhang et al., 2013) is well known for diacids. While some studies have probed a possible odd-even alternation in their reactivity with HO_2 (Taketani et al., 2013), NO_3 (de Semainville et al., 2010), and N_2O_5 (Griffiths et al., 2009), as well as in their TiO_2-based photocatalytic degradation (Sun et al.,

2014), extensive investigations of differences in chemical reactivity between odd and even diacids with amines have not been carried out.

The alternating behaviors between odd and even diacids have generally been attributed to the differences in their crystal structures. For example, odd-carbon diacids have higher aqueous solubility than even-carbon diacids because of the energetically unfavorable and looser crystal packing for the former, which facilitates penetration of water molecules between the molecular planes to dissolve the crystal (Zhang et al., 2013). It is possible that small amines, like water molecules, can also disrupt the crystal lattice of odd-carbon diacids more readily than that of the even-carbon species, thus leading to the observed odd-even alternation in the chemical reactivity. This may also explain why uptake of TMA is significantly smaller than BA (Fig. 2), where the bulky TMA structure may hinder the penetration and disruption of the acid crystal lattice. A similar steric effect has also been reported by Liu et al. (Liu et al., 2012) to explain the trends in reactivity on citric acid and humic acid particles of methylamine, dimethylamine, and TMA, which decreases with an increasing number of methyl groups.

Alternatively, the odd-even differences could be due to differences in surface composition and structure. Ruehl and Wilson (Ruehl and Wilson, 2014) observed an odd-even alternation in the hygroscopic growth of aqueous ammonium sulfate particles with a diacid shell. They attributed this behavior to the differences in the surface orientation of odd and even diacids on aqueous droplets, i.e., the "end to end" alignment with only one carboxyl group in contact with the aqueous phase for odd-carbon diacids versus the "folded" arrangement with both carboxyl groups in contact with the aqueous phase for the even-carbon acids. If a similar effect is present in the solids, an odd-even alternation in the reactivity with amines could result due to differences in surface availability of the –COOH groups.

Based on previous work by Lavi et al. (Lavi et al., 2015) the diacid and their alkylaminium salts vaporize well below 100 ^{o}C . Thus, in some experiments, the amine-reacted diacid particles were heated after exiting the 10-cm monolith denuder and prior to entering the DART-MS ionization region to probe whether the amine was distributed throughout the bulk of the particle or segregated on the surface. As seen in Fig. 3, there is no obvious temperature dependence, indicating that all of the amines in the particles are being sampled under all conditions. One explanation is that the entire particle is being sampled. Alternatively, if the amine reactions are

restricted to a surface layer as is common for gas-solid interactions, then the surface layer being probed at all T_{PS} is sufficiently deep to detect the entire particle-bound base. We show in the following that the latter is the likely explanation.

The molar ratio of amine to diacid ($R_{B/A}$) in amine-reacted diacid particles was estimated by comparing the DART-MS signal intensity ratio of amine to diacid measured at T_{PS} = 23 ^{o}C with that for known amine-diacid standard solutions (Fig. S5). As listed in Table 1, the $R_{B/A}$ values follow a similar trend as F_p (Fig. 2) for TMA- and BA-reacted malonic acid (C_3) and glutaric acid (C_5) particles.

However, the value of $R_{B/A}$ for BA-reacted pimelic acid (C_7) particles is larger than that for BA-reacted glutaric acid and malonic acid, inconsistent with the trend in F_p. A possible explanation can be suggested based on differences in the relative saturation vapor pressures (P_{sat}) (Bilde et al., 2015) of these diacids. It has been shown that the probe depth of online DART-MS is positively correlated with the volatility of straight chain even-diacid particles (Chan et al., 2013). Given that the volatility of C_7 (P_{sat} = 1.1 × 10^{-10} atm) is substantially lower than that of both C_3 and C_5 which are ~1.7 × 10^{-9} atm, the probe depth for C_7 particles is expected to be significantly smaller than the other two diacid particles, i.e., about a factor of 8 if the probe depth-volatility relationship reported for the even-diacid particles is extrapolated to the odd-diacids (Fig. S8). Correcting for this, the $R_{B/A}$ value would be about a factor of 8 smaller, i.e., ~ 0.05, which would follow the trend for the F_p values for all three amine-reacted odd-diacid particles. Note that although the probe depth may be smaller for C_7, the F_p value (Fig. 2) for the BA reaction suggests that it is still sufficient to detect all of the particle-bound amine (Fig. 3).

Comment [b9]: reworded for clarity

Comment [b10]: two word changes for clarity

3.1.2 Comparison with HR-ToF-AMS data

The $R_{B/A}$ values for TMA-reacted C_3 and C_5 diacid particles were also measured using HR-ToF-AMS and are shown in Table 1 and Fig. S7. The $R_{B/A}$ values for malonic acid and glutaric acid particles measured by HR-ToF-AMS are smaller than the corresponding values determined by DART-MS. The interaction between amines and carboxylic acids forms aminium carboxylate salts (Liu et al., 2012;Angelino et al., 2001;Lavi et al., 2015;Gomez-Hernandez et al., 2016), so that the gas-solid reaction is expected to form a surface layer of the salt. However, HR-ToF-AMS measures the entire particle (i.e., both the surface reacted layer and the unreacted bulk).

The larger $R_{B/A}$ values from DART-MS show that it is probing the reacted surface layer containing the aminium salt, plus perhaps some fraction of the underlying diacid. This is consistent with other studies where DART-MS was shown to probe mainly the surface layer (Chan et al., 2013;Nah et al., 2013).

In addition to direct measurements by HR-ToF-AMS, the $R_{B/A}$ values for the entire amine-reacted diacid particles can also be estimated by combining DART-MS with SMPS data. The number of amine molecules in the particles per cm^3 air ($N_{p\text{-}amine}$, molecules cm^{-3} air, Table S2) can be derived from Eq. (3),

$$N_{p-amine} = F_p \times N_{total} \quad (3)$$

where F_p is as defined in Eq. (2) above and N_{total} is the amount of amines in the gas phase plus those bound to the particles (molecules cm^{-3}) estimated from the DART-MS signal for the total amines and the DART-MS sensitivity to amines calibrated using gas phase amines with known concentrations generated as described in the experimental section. The number of diacid molecules in the particles per cm^3 air ($N_{p\text{-}acid}$) can be estimated from Eq. (4),

$$N_{p-acid} = \frac{[(V_p \times \rho) - m_{p-amine}] \times N_A}{MW_{acid}} \quad (4)$$

where V_p is the total volume concentration of amine-reacted diacid particles measured by SMPS (cm^3 particle volume per cm^{-3} air); ρ is the density of amine-reacted diacid particles, which is assumed to be the same as the solid diacid samples (i.e., 1.619 g cm^{-3} for malonic acid, 1.429 g cm^{-3} for glutaric acid, and 1.329 g cm^{-3} for pimelic acid (Lide, 2004)); $m_{p\text{-}amine}$ is the mass concentration of particle phase amines (g cm^{-3} air), which can be determined from Eq. (3); MW_{acid} is the molecular weight of the corresponding diacid (g mol^{-1}); and N_A is Avogadro's number.

Comment [b11]: units added to each number, removed from two lines up

The $R_{B/A}$ values calculated from the ratio of $N_{p\text{-}amine}$ to $N_{p\text{-}acid}$ are presented in Table 1. They are significantly smaller than those directly determined by DART-MS, further confirming that DART-MS mainly probes the surface layer of particles, and that the amines are segregated at the surface.

However, the calculated values are also smaller than the values measured by HR-ToF-AMS.

This is likely because the densities of the pure diacids were used in the calculations. Salts formed by reaction of amines with diacids tend to have densities that are smaller by as much as ~30% (Lavi et al., 2015). Small decreases in particle density would decrease the calculated particle mass concentrations and $N_{p\text{-}acid}$ (Eq. (4)), and hence increase calculated $R_{B/A}$ values. Despite the difference in the absolute values of $R_{B/A}$, the trends in $R_{B/A}$ values for TMA-reacted malonic acid and glutaric acid particles derived by DART-MS, HR-ToF-AMS, and calculations are consistent within the experimental uncertainty.

3.1.3 Estimation of probe depth for TMA-reacted odd diacid particles

When an amine reacts with a diacid, the resulting particle with radius R, is assumed to contain a diacid core (r_1), and an aminium salt shell of thickness $L_{shell} = (R - r_1)$ as shown in Fig. 4. The total volume of the particle, assuming a spherical geometry, can be expressed as:

$$V_{total} = \frac{4}{3}\pi R^3 \quad (5)$$

V_{total} can be obtained directly from SMPS data (Table S1). Since the total particle is comprised of the acid core and aminium salt shell, the total volume can also be expressed as,

$$V_{total} = V_s + V_c \quad (6)$$

where V_c is the volume of the acid core and V_s is the volume of the aminium salt shell. The volume of the shell can be obtained from the experimental data as follows:

$$V_s = \frac{m_s}{\rho_s} = \frac{n_s MW_s}{\rho_s} \quad (7)$$

In Eq. (7), m_s is the mass of the aminium salt, ρ_s is the density of the salt, n_s is the number of moles of salt per cm^3 air, and MW_s is the molecular weight of the aminium salt. Note that two values of V_s can be calculated if aminium salt forms with stoichiometric molar amine:acid ratios of either 1:1 or 2:1. In addition, the densities of the aminium salts are reported to be less than that of the pure acid, as much as ~30% lower for the 2:1 salt (Lavi et al., 2015). For the calculations below, the density of the salt is taken to be either 15% smaller than the acid for a 1:1 base-to-acid salt or 30% smaller for the 2:1 salt.

Thus, one can solve for r_1 as follows:

$$\frac{R}{r_1} = \left(\frac{V_{total}}{V_{core}}\right)^{\frac{1}{3}} = \left(\frac{V_{total}}{V_{total} - V_s}\right)^{\frac{1}{3}} \quad (8)$$

Using the volume weighted geometric mean diameter (nm) (Table S1) in Eq. (8) to obtain R, the radius of the acid core, r_1, as well as the thickness of the salt layer, L_{shell} ($L_{shell} = R - r_1$) can be obtained. Table 2 summarizes the results for TMA-reacted malonic acid and glutaric acid particles.

The probe depth (L_{DART}) is assumed to be comprised of the aminium salt shell (shaded red area) and some fraction of the acid core (shaded green area) (Fig. 4). The thickness of the aminium salt layer determined previously (L_{shell}) along with the ratio of $R_{B/A}$ values for a given diacid derived by DART-MS and HR-ToF-AMS (Table 1) can be used to estimate the probe depth of the reacted particles in the following manner.

As discussed earlier, the independence of F_p on particle stream temperature (T_{ps}) (Fig. 3) suggests that DART-MS probes all of the aminium salt shell plus likely *some* of the pure acid core. On the other hand, HR-ToF-AMS (by measuring the entire particles) probes the total amount of the amine present in the particles and *all* of the pure acid core. Thus, the ratio of the $R_{B/A}$ values from DART-MS to that of the HR-ToF-AMS can be expressed as:

$$\frac{R_{B/A,DART}}{R_{B/A,AMS}} = \frac{\frac{moles\ B(DART)}{moles\ A(DART)}}{\frac{moles\ B(AMS)}{moles\ A(AMS)}} = \frac{moles\ A(AMS)}{moles\ A(DART)} \quad (9)$$

The total volume of a particle can be expressed as a function of the different areas labelled in Fig. 4 as,

$$V_{total} = V_s + V_m + V_{uc} \quad (10)$$

where, V_s, V_m and V_{uc} are the volume of the salt shell (shaded red area), the volume of the middle layer (i.e. the volume of the acid core that is probed by DART-MS, shaded green area) and the volume of the core that is not probed by DART (yellow area) respectively (V_{uc} = unprobed core). While DART-MS is assumed to probe the salt layer and some fraction of the acid core, the HR-ToF-AMS will probe the entire bulk of the particle. As a result, Eq. (9) can be expressed as follows,

$$\frac{R_{B/A,DART}}{R_{B/A,AMS}} = \frac{\frac{\rho_s V_s}{MW_s} + \frac{\rho_A V_m}{MW_A} + \frac{\rho_A V_{uc}}{MW_A}}{\frac{\rho_s V_s}{MW_s} + \frac{\rho_A V_m}{MW_A}} \quad (11)$$

where ρ_s and MW_s are the density and molecular weight for the aminium salt, ρ_A and MW_A are the density and molecular weight of the diacid contained in the 'middle' layer and the acid core that is not probed by DART-MS.

The ratio of the base-to-acid molar ratio from DART-MS to that of the HR-ToF-AMS is ~2 (Table 1). As such, Eq. (11) can be simplified to yield Eq. (12):

$$\frac{\rho_s V_s}{MW_s} + \frac{\rho_A V_m}{MW_A} = \frac{\rho_A V_{uc}}{MW_A} \quad (12)$$

The spherical volumes of each section of the particle can now be expressed in terms of their respective radii based on Fig. 4:

$$\frac{\rho_s (R^3 - r_1^3)}{MW_s} + \frac{\rho_A (r_1^3 - r_2^3)}{MW_A} = \frac{\rho_A r_2^3}{MW_A} \quad (13)$$

The values of r_2 corresponding to a stoichiometric molar amine:acid ratio of 1:1 or 2:1 can then be derived along with the derived probe depth for DART-MS, $L_{DART} = (R - r_2)$. As can be seen in Table 2, using the volume weighted geometric mean diameter for the TMA-reacted malonic acid of 290 nm (Table S1), the decrease in the DART-MS ratio of $R_{B/A}$ from 0.28 to 0.14 for HR-ToF-AMS is consistent with a probe depth of ~ 32 nm, and is similar for glutaric acid, ~28 nm. It is worth noting that the values obtained for r_2 and L_{DART} are essentially independent of the assumed stoichiometry and would yield the same value for any mixture of 1:1 and 2:1 salt.

3.2 Characterization of α-cedrene SOA particles

In earlier studies (Zhao et al., 2016), limited DART-MS measurements were made for SOA particles at T_{PS} = 160 ^{o}C from the ozonolysis of α-cedrene for purposes of confirming high molecular weight (HMW) products identified in ESI mass spectra. More extensive measurements were carried out here to investigate in more detail the application of DART-MS to organic particles of complex composition. Figure 5 shows DART(-) (negative ion mode) mass spectra of polydisperse α-cedrene SOA particles measured as a function of T_{PS} for distributions

with different $\bar{D}_{g,S}$, 21 nm and 28 nm. The ion signals observed in the mass spectra of SOA particles at T_{PS} = 23 ^{o}C (Figs. 5a and 5c) are dominated by low molecular weight (LMW) products (*m/z* 200-350), with a small contribution from HMW products (*m/z* 420-580). This is not surprising given the very short particle residence time in the ionization region (estimated to be of the order of milliseconds under our conditions), which limits the vaporization of low volatility HMW products from SOA particles. However, the signal intensities of HMW products as well as most of the LMW products increase substantially at T_{PS} = 125 ^{o}C (Figs. 5b and 5d). It is not known if the entire particle is vaporized at this temperature, although essentially complete vaporization has been reported for larger SOA particles precursors (Kolesar et al., 2015). Many of the LMW products in α-cedrene SOA particles observed in DART mass spectra were also detected using GC-MS (Jaoui et al., 2004;Yao et al., 2014;Jaoui et al., 2013) and APCI-MS (Reinnig et al., 2009) in other studies. The possible structures and formation mechanism of many of these LMW products were investigated in previous studies (Jaoui et al., 2004;Reinnig et al., 2009;Jaoui et al., 2013;Yao et al., 2014;Zhao et al., 2016) and those for HMW products in our previous study (Zhao et al., 2016).

Potential artifacts in DART-MS with respect to in-source oxidation chemistry and gas phase ion clustering of organic compounds that forms non-covalently bound HMW species were evaluated by analyzing different organic standards and α-cedrene SOA particles in the negative ion mode under varying controlled conditions. Details of the analysis and results can be found in Section 8 of the SI. The results show that measurements of diacid particles and α-cedrene SOA particles with DART-MS do not suffer from in-source oxidation and gas phase clustering artifacts.

Differences in DART mass spectra of α-cedrene SOA particles at T_{PS} = 23 ^{o}C or 125 ^{o}C in Fig. 5 are consistent with a dependence of product distribution on particle size as reported earlier based on ESI-MS (Zhao et al., 2016). To better explore the size- and temperature-dependent product distribution in α-cedrene SOA particles, the intensity ratio of HMW to LMW products as well as the intensity fraction of the two prominent LMW products, i.e., *m/z* 253 and *m/z* 267, was examined as a function of T_{PS} and particle size. Figure 6a shows the signal intensity ratio of HMW products (summed over *m/z* 420-580) to that of LMW products (summed over *m/z* 200-350) for α-cedrene SOA particles with a $\bar{D}_{g,S}$ of 21 nm and 28 nm at different T_{PS}. Smaller particles at each T_{PS} show a greater contribution from HMW products to the total ion signal,

consistent with these products serving as important agents for initial particle formation (Zhao et al., 2016).

In our previous study (Zhao et al., 2016), HR-ToF-AMS was used to characterize the bulk composition of α-cedrene ozonolysis particles generated in Teflon chambers. Under dry conditions (<5%), chamber-generated particles had an O:C = 0.34, which was characteristic of LMW products that were shown to contribute primarily to particle growth rather than to initial particle formation. This is not necessarily surprising since the chamber-generated particles had undergone significantly more particle growth ($\overline{D}_{g,N}$~70 nm) than particles generated in the flow reactor ($\overline{D}_{g,N}$ < 30 nm), which are too small to transmit through the HR-ToF-AMS lens. While bulk particle composition measurements by AMS were limited to chamber particles, their comparison to DART-MS measurements show that LMW components make up the majority of the particle mass at long reaction times. This highlights the value of DART-MS in accessing the markedly different compositions at varied extent of particle growth.

Figure 6b shows the intensity fraction of products with peaks at *m/z* 253 or *m/z* 267 to the total LMW products (*m/z* 200-350) at different T_{PS} for polydisperse α-cedrene SOA particles with distributions having a $\overline{D}_{g,S}$ centered at 21 nm and 28 nm, respectively. For both distributions, the fraction of product *m/z* 253 increases with rising T_{PS} whereas that of product *m/z* 267 decreases with increasing T_{PS}. The distinct temperature dependence of these two peaks may indicate that the product responsible for *m/z* 253 has a lower volatility than product *m/z* 267 (although a contribution from decomposition of HMW products at higher T_{PS} cannot be ruled out). Smaller particles tend to have a greater fraction of *m/z* 253 compared to larger particles but a lower fraction from *m/z* 267. This suggests that the species responsible for *m/z* 253 play a more important role in the early stages of particle growth, consistent with its lower volatility. Previous studies have proposed multiple isomeric structures, i.e., α-cedrinic acid and 10-hydroxy-α-norcedralic acid for product *m/z* 253 (Jaoui et al., 2004;Reinnig et al., 2009;Jaoui et al., 2013;Yao et al., 2014;Zhao et al., 2016). Using the EVAPORATION model (Compernolle et al., 2011), the P_{sat} of α-cedrinic acid and 10-hydroxy-α-norcedralic acid are estimated to be 2.4×10^{-12} atm and 5.1×10^{-11} atm, respectively, and the P_{sat} of the structures proposed for *m/z* 267 is estimated to be $(0.39\text{-}3.1) \times 10^{-11}$ atm (Zhao et al., 2016). Therefore, α-cedrinic acid, the P_{sat} of which is lower than all possible isomeric structures of *m/z* 263, is likely the dominant structure for the product

m/z 253. This illustrates that DART-MS measurements may help resolve structural isomers of some products by providing information on their volatility.

4. Conclusions

DART-MS was successfully applied to the real-time study of the reaction of submicron diacid particles with gas phase amines and to the chemical composition of nanometer-sized SOA particles from ozonolysis of α-cedrene. The reactivity of C_3-C_7 diacid particles toward TMA and BA exhibits a clear alternation between the odd and even carbon numbers. Calibrations using known amine-diacid mixtures enable the determination of the ratios of the base to acid in reacted particles. The relative increase in these ratios for DART-MS compared to those derived by HR-ToF-MS was used to estimate the probe depth of DART-MS. It is shown that DART-MS probes mainly the surface layer of the particles, in agreement with other studies on different systems. Results for α-cedrene SOA particles show that HMW products are a major component of the smaller particles, consistent with these products playing an important role in initial particle formation (Zhao et al., 2016). Vaporization of particles at different temperatures before introduction into the DART ionization region permits the characterization of isomeric structures of SOA particles based on their volatility. All of these studies were carried out under dry conditions. The presence of water vapor would be expected to influence some of the physical and chemical processes involved in both systems. This remains to be investigated.

Some challenges remain in applying DART-MS, for example quantification of individual compounds. While relative concentrations can be determined by utilizing an internal (Zhou et al., 2015;Schilling Fahnestock et al., 2015) or external standard (as shown for the amine-diacid system in our present study), this assumes that DART-MS has the same sensitivity for the standards and the analytes. This might not hold for SOA particles that consist of a complex mixture of organic compounds with a wide diversity of functionality and polarity. In addition, internal standards need to be well-mixed with the sample, which can be difficult if the standard and analyte recrystallize separately. Furthermore, the standard configuration for DART-MS at present operates in an open environment so the amount of the analyte actually sampled by the MS may not be well controlled. As with many other ambient ionization techniques, caution is warranted with respect to possible oxidation by OH and other reactive species generated in the source.

However, this study in combination with previous work (Nah et al., 2013;Chan et al., 2013;Zhou et al., 2015;Schilling Fahnestock et al., 2015;Chan et al., 2014;Davies and Wilson, 2015;Zhao et al., 2016) demonstrates that DART-MS is a very useful complement to ESI-MS and other mass spectrometric techniques for the analysis of complex atmospherically relevant systems. Combined with temperature studies, it can provide depth information on spatially heterogeneous particles and potentially differentiate between isobaric compounds of different volatility.

Acknowledgements

This work was supported by the National Science Foundation (Grants #1207112, #1404233 and #1443140) and the NSF Major Research Instrumentation (MRI) program (Grants #1337080 and #0923323). The authors would like to thank Kristine Arquero for assistance with the TMA permeation tube and measurements of the gas phase TMA concentration.

References

Aljawhary, D., Lee, A. K. Y., and Abbatt, J. P. D.: High-resolution chemical ionization mass spectrometry (ToF-CIMS): application to study SOA composition and processing, Atmos. Meas. Tech., 6, 3211-3224, 2013.

Angelino, S., Suess, D. T., and Prather, K. A.: Formation of aerosol particles from reactions of secondary and tertiary alkylamines: characterization by aerosol time-of-flight mass spectrometry, Environ. Sci. Technol., 35, 3130-3138, 2001.

Bilde, M., Svenningsson, B., Monster, J., and Rosenorn, T.: Even-odd alternation of evaporation rates and vapor pressures of C_3-C_9 dicarboxylic acid aerosols, Environ. Sci. Technol., 37, 1371-1378, 2003.

Bilde, M., Barsanti, K., Booth, M., Cappa, C. D., Donahue, N. M., Emanuelsson, E. U., McFiggans, G., Krieger, U. K., Marcolli, C., Tropping, D., Ziemann, P., Barley, M., Clegg, S., Dennis-Smither, B., Hallquist, M., Hallquist, A. M., Khlystov, A., Kulmala, M., Mogensen, D., Percival, C. J., Pope, F., Reid, J. P., da Silva, M. A. V. R., Rosenoern, T., Salo, K., Soonsin, V. P., Yli-Juuti, T., Prisle, N. L., Pagels, J., Rarey, J., Zardini, A. A., and Riipinen, I.: Saturation vapor pressures and transition enthalpies of low-volatility organic molecules of atmospheric relevance: from dicarboxylic acids to complex mixtures, Chem. Rev., 115, 4115-4156, 2015.

Bruns, E. A., Greaves, J., and Finlayson-Pitts, B. J.: Measurement of vapor pressures and heats of sublimation of dicarboxylic acids using atmospheric solids analysis probe mass spectrometry, J. Phys. Chem. A., 116, 5900-5909, 2012.

Bzdek, B. R., Lawler, M. J., Horan, A. J., Pennington, M. R., DePalma, J. W., Zhao, J., Smith, J. N., and Johnston, M. V.: Molecular constraints on particle growth during new particle formation, Geophys. Res. Lett., 41, 6045-6054, 2014.

Canagaratna, M. R., Jimenez, J. L., Kroll, J. H., Chen, Q., Kessler, S. H., Massoli, P., Ruiz, L. H., Fortner, E., Williams, L. R., Wilson, K. R., Surratt, J. D., Donahue, N. M., Jayne, J. T., and Worsnop, D. R.: Elemental ratio measurements of organic compounds using aerosol mass spectrometry: characterization, improved calibration, and implications, Atmos. Chem. Phys., 15, 253-272, 2015.

Cappa, C. D., Lovejoy, E. R., and Ravishankara, A. R.: Determination of evaporation rates and vapor pressures of very low volatility compounds: a study of the C_4-C_{10} and C_{12} dicarboxylic acids, J. Phys. Chem. A., 111, 3099-3109, 2007.

Chan, M. N., Nah, T., and Wilson, K. R.: Real time *in situ* chemical characterization of sub-micron organic aerosols using direct analysis in real time mass spectrometry (DART-MS): the effect of aerosol size and volatility, Analyst, 138, 3749-3757, 2013.

Chan, M. N., Zhang, H. F., Goldstein, A. H., and Wilson, K. R.: Role of water and phase in the heterogeneous oxidation of solid and aqueous succinic acid aerosol by hydroxyl radicals, J. Phys. Chem. C., 118, 28978-28992, 2014.

Chen, H., Venter, A., and Cooks, R. G.: Extractive electrospray ionization for direct analysis of undiluted urine, milk and other complex mixtures without sample preparation, Chem. Commun., 2042-2044, 2006.

Chen, H., Sun, Y., Wortmann, A., Gu, H., and Zenobi, R.: Differentiation of maturity and quality of fruit using noninvasive extractive electrospray ionization quadrupole time-of-flight mass spectrometry, Anal. Chem., 79, 1447-1455, 2007.

Chen, H., Varner, M. E., Gerber, R. B., and Finlayson-Pitts, B. J.: Reactions of methanesulfonic acid with amines and ammonia as a source of new particles in air, J. Phys. Chem. B., 120,

1526-1536, 2016.
Chingin, K., Gamez, G., Chen, H., Zhu, L., and Zenobi, R.: Rapid classification of perfumes by extractive electrospray ionization mass spectrometry (EESI-MS), Rapid Commun. Mass. Sp., 22, 2009-2014, 2008.
Cody, R. B., Laramee, J. A., and Durst, H. D.: Versatile new ion source for the analysis of materials in open air under ambient conditions, Anal. Chem., 77, 2297-2302, 2005.
Compernolle, S., Ceulemans, K., and Muller, J. F.: EVAPORATION: a new vapour pressure estimation method for organic molecules including non-additivity and intramolecular interactions, Atmos. Chem. Phys., 11, 9431-9450, 2011.
Davies, J. F., and Wilson, K. R.: Nanoscale interfacial gradients formed by the reactive uptake of OH radicals onto viscous aerosol surfaces, Chem. Sci., 6, 7020-7027, 2015.
Dawson, M. L., Varner, M. E., Perraud, V., Ezell, M. J., Gerber, R. B., and Finlayson-Pitts, B. J.: Simplified mechanism for new particle formation from methanesulfonic acid, amines, and water via experiments and *ab initio* calculations, P. Natl. Acad. Sci. USA., 109, 18719-18724, 2012.
Dawson, M. L., Perraud, V., Gomez, A., Arquero, K. D., Ezell, M. J., and Finlayson-Pitts, B. J.: Measurement of gas-phase ammonia and amines in air by collection onto an ion exchange resin and analysis by ion chromatography, Atmos. Meas. Tech., 7, 2733-2744, 2014.
De Haan, D. O., Hawkins, L. N., Kononenko, J. A., Turley, J. J., Corrigan, A. L., Tolbert, M. A., and Jimenez, J. L.: Formation of nitrogen-containing oligomers by methylglyoxal and amines in simulated evaporating cloud droplets, Environ. Sci. Technol., 45, 984-991, 2011.
de Semainville, P. G., D'Anna, B., and George, C.: Aqueous phase reactivity of nitrate radicals (NO_3) toward dicarboxylic acids, Z. Phys. Chem., 224, 1247-1260, 2010.
DeCarlo, P. F., Kimmel, J. R., Trimborn, A., Northway, M. J., Jayne, J. T., Aiken, A. C., Gonin, M., Fuhrer, K., Horvath, T., Docherty, K. S., Worsnop, D. R., and Jimenez, J. L.: Field-deployable, high-resolution, time-of-flight aerosol mass spectrometer, Anal. Chem., 78, 8281-8289, 2006.
Doezema, L., Longin, T., Cody, W., Perraud, V., Dawson, M. L., Ezell, M. J., Greaves, J., Johnson, K. R., and Finlayson-Pitts, B. J.: Analysis of secondary organic aerosols in air using extractive electrospray ionization mass spectrometry (EESI-MS) RSC Adv., 2, 2930-2938, 2012.
Duporte, G., Parshintsev, J., Barreira, L. M. F., Hartonen, K., Kulmala, M., and Riekkola, M. L.: Nitrogen-containing low volatile compounds from pinonaldehyde-dimethylamine reaction in the atmosphere: A laboratory and field study, Environ. Sci. Technol., 4693–4700, 2016.
Ervens, B., Turpin, B. J., and Weber, R. J.: Secondary organic aerosol formation in cloud droplets and aqueous particles (aqSOA): a review of laboratory, field and model studies, Atmos. Chem. Phys., 11, 11069-11102, 2011.
Farmer, D. K., Cappa, C. D., and Kreidenweis, S. M.: Atmospheric processes and their controlling influence on cloud condensation nuclei activity, Chem. Rev., 115, 4199-4217, 2015.
Finlayson-Pitts, B. J., and Pitts, J. N.: Chemistry of the Upper and Lower Atmosphere : Theory, Experiments, and Applications, Academic Press, San Diego, 2000.
Gallimore, P. J., and Kalberer, M.: Characterizing an extractive electrospray ionization (EESI)

source for the online mass spectrometry analysis of organic aerosols, Environ. Sci. Technol., 47, 7324-7331, 2013.
Gao, Y. Q., Hall, W. A., and Johnston, M. V.: Molecular composition of monoterpene secondary organic aerosol at low mass loading, Environ. Sci. Technol., 44, 7897-7902, 2010.
Gard, E., Mayer, J. E., Morrical, B. D., Dienes, T., Fergenson, D. P., and Prather, K. A.: Real-time analysis of individual atmospheric aerosol particles: design and performance of a portable ATOFMS, Anal. Chem., 69, 4083-4091, 1997.
Ge, X. L., Wexler, A. S., and Clegg, S. L.: Atmospheric amines - part I. A review, Atmos. Environ., 45, 524-546, 2011.
George, C., Ammann, M., D'Anna, B., Donaldson, D. J., and Nizkorodov, S. A.: Heterogeneous Photochemistry in the Atmosphere, Chem. Rev., 115, 4218-4258, 2015.
Glasius, M., and Goldstein, A. H.: Recent discoveries and future challenges in atmospheric organic chemistry, Environ. Sci. Technol., 50, 2754−2764, 2016.
Gomez-Hernandez, M., McKeown, M., Secrest, J., Marrero-Ortiz, W., Lavi, A., Rudich, Y., Collins, D. R., and Zhang, R. Y.: Hygroscopic characteristics of alkylaminium carboxylate aerosols, Environ. Sci. Technol., 50, 2292-2300, 2016.
Griffiths, P. T., Badger, C. L., Cox, R. A., Folkers, M., Henk, H. H., and Mentel, T. F.: Reactive uptake of N_2O_5 by aerosols containing dicarboxylic acids. Effect of particle phase, composition, and nitrate content, J. Phys. Chem. A., 113, 5082-5090, 2009.
Gross, J. H.: Direct analysis in real time-a critical review on DART-MS, Anal. Bioanal. Chem., 406, 63-80, 2014.
Hallquist, M., Wenger, J. C., Baltensperger, U., Rudich, Y., Simpson, D., Claeys, M., Dommen, J., Donahue, N. M., George, C., Goldstein, A. H., Hamilton, J. F., Herrmann, H., Hoffmann, T., Iinuma, Y., Jang, M., Jenkin, M. E., Jimenez, J. L., Kiendler-Scharr, A., Maenhaut, W., McFiggans, G., Mentel, T. F., Monod, A., Prevot, A. S. H., Seinfeld, J. H., Surratt, J. D., Szmigielski, R., and Wildt, J.: The formation, properties and impact of secondary organic aerosol: current and emerging issues, Atmos. Chem. Phys., 9, 5155-5236, 2009.
Herrmann, H., Schaefer, T., Tilgner, A., Styler, S. A., Weller, C., Teich, M., and Otto, T.: Tropospheric aqueous-phase chemistry: kinetics, mechanisms, and its coupling to a changing gas phase, Chem. Rev., 115, 4259-4334, 2015.
Horan, A. J., Gao, Y. Q., Hall, W. A., and Johnston, M. V.: Online characterization of particles and gases with an ambient electrospray ionization source, Anal. Chem., 84, 9253-9258, 2012.
Huey, L. G.: Measurement of trace atmospheric species by chemical ionization mass spectrometry: speciation of reactive nitrogen and future directions, Mass. Spectrom. Rev., 26, 166-184, 2007.
Jackson, A. U., Werner, S. R., Talaty, N., Song, Y., Campbell, K., Cooks, R. G., and Morgan, J. A.: Targeted metabolomic analysis of Escherichia coli by desorption electrospray ionization and extractive electrospray ionization mass spectrometry, Anal. Biochem., 375, 272-281, 2008.
Jaoui, M., Sexton, K. G., and Kamens, R. M.: Reaction of α-cedrene with ozone: mechanism, gas and particulate products distribution, Atmos. Environ., 38, 2709-2725, 2004.
Jaoui, M., Kleindienst, T. E., Docherty, K. S., Lewandowski, M., and Offenberg, J. H.: Secondary organic aerosol formation from the oxidation of a series of sesquiterpenes: α-cedrene, β-caryophyllene, α-humulene and α-farnesene with O_3, OH and NO_3 radicals, Environ. Chem., 10, 178-193, 2013.

Jimenez, J. L., Canagaratna, M. R., Donahue, N. M., Prevot, A. S. H., Zhang, Q., Kroll, J. H., DeCarlo, P. F., Allan, J. D., Coe, H., Ng, N. L., Aiken, A. C., Docherty, K. S., Ulbrich, I. M., Grieshop, A. P., Robinson, A. L., Duplissy, J., Smith, J. D., Wilson, K. R., Lanz, V. A., Hueglin, C., Sun, Y. L., Tian, J., Laaksonen, A., Raatikainen, T., Rautiainen, J., Vaattovaara, P., Ehn, M., Kulmala, M., Tomlinson, J. M., Collins, D. R., Cubison, M. J., Dunlea, E. J., Huffman, J. A., Onasch, T. B., Alfarra, M. R., Williams, P. I., Bower, K., Kondo, Y., Schneider, J., Drewnick, F., Borrmann, S., Weimer, S., Demerjian, K., Salcedo, D., Cottrell, L., Griffin, R., Takami, A., Miyoshi, T., Hatakeyama, S., Shimono, A., Sun, J. Y., Zhang, Y. M., Dzepina, K., Kimmel, J. R., Sueper, D., Jayne, J. T., Herndon, S. C., Trimborn, A. M., Williams, L. R., Wood, E. C., Middlebrook, A. M., Kolb, C. E., Baltensperger, U., and Worsnop, D. R.: Evolution of organic aerosols in the atmosphere, Science, 326, 1525-1529, 2009.

Kawamura, K., and Bikkina, S.: A review of dicarboxylic acids and related compounds in atmospheric aerosols: molecular distributions, sources and transformation, Atmos. Res., 170, 140-160, 2016.

Kolesar, K. R., Li, Z. Y., Wilson, K. R., and Cappa, C. D.: Heating-induced evaporation of nine different secondary organic aerosol types, Environ. Sci. Technol., 49, 12242-12252, 2015.

Kroll, J. H., and Seinfeld, J. H.: Chemistry of secondary organic aerosol: formation and evolution of low-volatility organics in the atmosphere, Atmos. Environ., 42, 3593-3624, 2008.

Kulmala, M., Petaja, T., Ehn, M., Thornton, J., Sipila, M., Worsnop, D. R., and Kerminen, V. M.: Chemistry of atmospheric nucleation: on the recent advances on precursor characterization and atmospheric cluster composition in connection with atmospheric new particle formation, Annu. Rev. Phys. Chem., 65, 21-37, 2014.

Laskin, A., Laskin, J., and Nizkorodov, S. A.: Mass spectrometric approaches for chemical characterisation of atmospheric aerosols: critical review of the most recent advances, Environ. Chem., 9, 163-189, 2012.

Laskin, A., Laskin, J., and Nizkorodov, S. A.: Chemistry of atmospheric brown carbon, Chem. Rev., 115, 4335-4382, 2015.

Laskin, J., Laskin, A., and Nizkorodov, S. A.: New mass spectrometry techniques for studying physical chemistry of atmospheric heterogeneous processes, Int. Rev. Phys. Chem., 32, 128-170, 2013.

Lavi, A., Segre, E., Gomez-Hernandez, M., Zhang, R. Y., and Rudich, Y.: Volatility of atmospherically relevant alkylaminium carboxylate salts, J. Phys. Chem. A., 119, 4336-4346, 2015.

Law, W. S., Wang, R., Hu, B., Berchtold, C., Meier, L., Chen, H. W., and Zenobi, R.: On the mechanism of extractive electrospray ionization, Anal. Chem., 82, 4494-4500, 2010.

Lide, D. R.: CRC Handbook of Chemistry and Physics, CRC press, 2004.

Liu, Y. C., Ma, Q. X., and He, H.: Heterogeneous uptake of amines by citric acid and humic acid, Environ. Sci. Technol., 46, 11112-11118, 2012.

Lopez-Hilfiker, F. D., Mohr, C., Ehn, M., Rubach, F., Kleist, E., Wildt, J., Mentel, T. F., Lutz, A., Hallquist, M., Worsnop, D., and Thornton, J. A.: A novel method for online analysis of gas and particle composition: description and evaluation of a filter inlet for gases and AEROsols (FIGAERO), Atmos. Meas. Tech., 7, 983-1001, 2014.

Moise, T., Flores, J. M., and Rudich, Y.: Optical properties of secondary organic aerosols and their changes by chemical processes, Chem. Rev., 115, 4400-4439, 2015.

699 Muller, C., Iinuma, Y., Karstensen, J., van Pinxteren, D., Lehmann, S., Gnauk, T., and Herrmann,
700 H.: Seasonal variation of aliphatic amines in marine sub-micrometer particles at the Cape
701 Verde islands, Atmos. Chem. Phys., 9, 9587-9597, 2009a.
702 Muller, L., Reinnig, M. C., Hayen, H., and Hoffmann, T.: Characterization of oligomeric
703 compounds in secondary organic aerosol using liquid chromatography coupled to
704 electrospray ionization Fourier transform ion cyclotron resonance mass spectrometry,
705 Rapid Commun. Mass. Sp., 23, 971-979, 2009b.
706 Murphy, D. M., and Thomson, D. S.: Laser ionization mass-spectroscopy of single aerosol-
707 particles, Aerosol Sci. Tech., 22, 237-249, 1995.
708 Nah, T., Chan, M., Leone, S. R., and Wilson, K. R.: Real time *in situ* chemical characterization
709 of submicrometer organic particles using direct analysis in real time-mass spectrometry,
710 Anal. Chem., 85, 2087-2095, 2013.
711 Ng, N. L., Canagaratna, M. R., Zhang, Q., Jimenez, J. L., Tian, J., Ulbrich, I. M., Kroll, J. H.,
712 Docherty, K. S., Chhabra, P. S., Bahreini, R., Murphy, S. M., Seinfeld, J. H., Hildebrandt,
713 L., Donahue, N. M., DeCarlo, P. F., Lanz, V. A., Prevot, A. S. H., Dinar, E., Rudich, Y.,
714 and Worsnop, D. R.: Organic aerosol components observed in Northern Hemispheric
715 datasets from aerosol mass spectrometry, Atmos. Chem. Phys., 10, 4625-4641, 2010.
716 Nizkorodov, S. A., Laskin, J., and Laskin, A.: Molecular chemistry of organic aerosols through
717 the application of high resolution mass spectrometry, Phys. Chem. Chem. Phys., 13,
718 3612-3629, 2011.
719 Noziere, B., Kaberer, M., Claeys, M., Allan, J., D'Anna, B., Decesari, S., Finessi, E., Glasius, M.,
720 Grgic, I., Hamilton, J. F., Hoffmann, T., Iinuma, Y., Jaoui, M., Kahnt, A., Kampf, C. J.,
721 Kourtchev, I., Maenhaut, W., Marsden, N., Saarikoski, S., Schnelle-Kreis, J., Surratt, J. D.,
722 Szidat, S., Szmigielski, R., and Wisthaler, A.: The molecular identification of organic
723 compounds in the atmosphere: state of the art and challenges, Chem. Rev., 115, 3919-
724 3983, 2015.
725 Powelson, M. H., Espelien, B. M., Hawkins, L. N., Galloway, M. M., and De Haan, D. O.:
726 Brown carbon formation by aqueous-phase carbonyl compound reactions with amines
727 and ammonium sulfate, Environ. Sci. Technol., 48, 985-993, 2014.
728 Pratt, K. A., and Prather, K. A.: Mass spectrometry of atmospheric aerosols-recent developments
729 and applications. Part 1: off-line mass spectrometry techniques, Mass. Spectrom. Rev., 31,
730 1-16, 2012a.
731 Pratt, K. A., and Prather, K. A.: Mass spectrometry of atmospheric aerosols-recent developments
732 and applications. Part 2: on-line mass spectrometry techniques, Mass. Spectrom. Rev., 31,
733 17-48, 2012b.
734 Reinnig, M. C., Warnke, J., and Hoffmann, T.: Identification of organic hydroperoxides and
735 hydroperoxy acids in secondary organic aerosol formed during the ozonolysis of different
736 monoterpenes and sesquiterpenes by on-line analysis using atmospheric pressure
737 chemical ionization ion trap mass spectrometry, Rapid Commun. Mass. Sp., 23, 1735-
738 1741, 2009.
739 Ruehl, C. R., and Wilson, K. R.: Surface organic monolayers control the hygroscopic growth of
740 submicrometer particles at high relative humidity, J. Phys. Chem. A., 118, 3952-3966,
741 2014.
742 Schilling Fahnestock, K. A., Yee, L. D., Loza, C. L., Coggon, M. M., Schwantes, R., Zhang, X.,
743 Dalleska, N. F., and Seinfeld, J. H.: Secondary organic aerosol composition from C_{12}
744 alkanes, J. Phys. Chem. A., 119, 4281-4297, 2015.

745 Smith, J. N., Moore, K. F., McMurry, P. H., and Eisele, F. L.: Atmospheric measurements of sub-
746 20 nm diameter particle chemical composition by thermal desorption chemical ionization
747 mass spectrometry, Aerosol Sci. Tech., 38, 100-110, 2004.
748 Sun, Y. R., Chang, W., Ji, H. W., Chen, C. C., Ma, W. H., and Zhao, J. C.: An unexpected
749 fluctuating reactivity for odd and even carbon numbers in the TiO_2-based photocatalytic
750 decarboxylation of C_2-C_6 dicarboxylic acids, Chem-Eur. J., 20, 1861-1870, 2014.
751 Taketani, F., Kanaya, Y., and Akimoto, H.: Kinetic studies of heterogeneous reaction of HO_2
752 radical by dicarboxylic acid particles, Int. J. Chem. Kinet., 45, 560-565, 2013.
753 Thalladi, V. R., Nusse, M., and Boese, R.: The melting point alternation in α,ω-
754 alkanedicarboxylic acids, J. Am. Chem. Soc., 122, 9227-9236, 2000.
755 Tobias, H. J., Kooiman, P. M., Docherty, K. S., and Ziemann, P. J.: Real-time chemical analysis
756 of organic aerosols using a thermal desorption particle beam mass spectrometer, Aerosol
757 Sci. Tech., 33, 170-190, 2000.
758 Wang, R., Grohn, A. J., Zhu, L., Dietiker, R., Wegner, K., Gunther, D., and Zenobi, R.: On the
759 mechanism of extractive electrospray ionization (EESI) in the dual-spray configuration,
760 Anal. Bioanal. Chem., 402, 2633-2643, 2012.
761 Winkler, P. M., Ortega, J., Karl, T., Cappellin, L., Friedli, H. R., Barsanti, K., McMurry, P. H.,
762 and Smith, J. N.: Identification of the biogenic compounds responsible for size-dependent
763 nanoparticle growth, Geophys. Res. Lett., 39, L20815, 2012.
764 Yao, L., Ma, Y., Wang, L., Zheng, J., Khalizov, A., Chen, M. D., Zhou, Y. Y., Qi, L., and Cui, F.
765 P.: Role of stabilized Criegee intermediate in secondary organic aerosol formation from
766 the ozonolysis of α-cedrene, Atmos. Environ., 94, 448-457, 2014.
767 Yatavelli, R. L. N., Lopez-Hilfiker, F., Wargo, J. D., Kimmel, J. R., Cubison, M. J., Bertram, T.
768 H., Jimenez, J. L., Gonin, M., Worsnop, D. R., and Thornton, J. A.: A chemical ionization
769 high-resolution time-of-flight mass spectrometer coupled to a micro orifice volatilization
770 impactor (MOVI-HR-ToF-CIMS) for analysis of gas and particle-phase organic species,
771 Aerosol Sci. Tech., 46, 1313-1327, 2012.
772 Zelenyuk, A., and Imre, D.: Single particle laser ablation time-of-flight mass spectrometer: an
773 introduction to SPLAT, Aerosol Sci. Tech., 39, 554-568, 2005.
774 Zhang, H., Xie, C., Liu, Z. K., Gong, J. B., Bao, Y., Zhang, M. J., Hao, H. X., Hou, B. H., and
775 Yin, Q. X.: Identification and molecular understanding of the odd-even effect of
776 dicarboxylic acids aqueous solubility, Ind. Eng. Chem. Res., 52, 18458-18465, 2013.
777 Zhang, Q., Jimenez, J. L., Canagaratna, M. R., Allan, J. D., Coe, H., Ulbrich, I., Alfarra, M. R.,
778 Takami, A., Middlebrook, A. M., Sun, Y. L., Dzepina, K., Dunlea, E., Docherty, K.,
779 DeCarlo, P. F., Salcedo, D., Onasch, T., Jayne, J. T., Miyoshi, T., Shimono, A.,
780 Hatakeyama, S., Takegawa, N., Kondo, Y., Schneider, J., Drewnick, F., Borrmann, S.,
781 Weimer, S., Demerjian, K., Williams, P., Bower, K., Bahreini, R., Cottrell, L., Griffin, R.
782 J., Rautiainen, J., Sun, J. Y., Zhang, Y. M., and Worsnop, D. R.: Ubiquity and dominance
783 of oxygenated species in organic aerosols in anthropogenically-influenced Northern
784 Hemisphere midlatitudes, Geophys. Res. Lett., 34, L13801, 2007.
785 Zhang, R. Y., Khalizov, A., Wang, L., Hu, M., and Xu, W.: Nucleation and growth of
786 nanoparticles in the atmosphere, Chem. Rev., 112, 1957-2011, 2012.
787 Zhao, Y., Wingen, L. M., Perraud, V., Greaves, J., and Finlayson-Pitts, B. J.: Role of the reaction
788 of stabilized Criegee intermediates with peroxy radicals in particle formation and growth
789 in air, Phys. Chem. Chem. Phys., 17, 12500-12514, 2015.
790 Zhao, Y., Wingen, L. M., Perraud, V., and Finlayson-Pitts, B. J.: Phase, composition, and growth

mechanism for secondary organic aerosol from the ozonolysis of α-cedrene, Atmos. Chem. Phys., 16, 3245-3264, 2016.
Zhou, S. M., Forbes, M. W., and Abbatt, J. P. D.: Application of direct analysis in real time-mass spectrometry (DART-MS) to the study of gas-surface heterogeneous reactions: focus on ozone and PAHs, Anal. Chem., 87, 4733-4740, 2015.
Ziemann, P. J., and Atkinson, R.: Kinetics, products, and mechanisms of secondary organic aerosol formation, Chem. Soc. Rev., 41, 6582-6605, 2012.

Table 1. $R_{B/A}$ values for amine-reacted malonic acid (C_3), glutaric acid (C_5), and pimelic acid (C_7) particles derived by DART-MS, HR-ToF-AMS, and calculations.

	$R_{B/A}$ (DART-MS)	$R_{B/A}$ (AMS)	Calculated $R_{B/A}$ from F_p and the particle size distributions[c]
TMA-C_3	0.28 ± 0.07	0.14 ± 0.01	0.07 ± 0.02
TMA-C_5	0.05 ± 0.02	0.03 ± 0.01	0.02 ± 0.003
TMA-C_7	—[a]	0.01 ± 0.001	—[a]
BA-C_3	0.40 ± 0.09	—[b]	0.09 ± 0.03
BA-C_5	0.22 ± 0.02	—[b]	0.07 ± 0.01
BA-C_7	0.42 ± 0.06	—[b]	0.07 ± 0.02

[a]No particle-bound amines were detected by DART-MS. [b]Measurements by AMS were not performed. [c]See Eq. (3) and (4) in text. Lower limit due to uncertainty in particle density as described in text.

807 **Table 2.** Thickness of the aminium salt shell and DART probe depth for trimethylamine (TMA)-
808 reacted malonic acid and glutaric acid.

	R (nm)	r_1 (nm)		r_2 (nm)		L_{shell} (nm)		L_{DART} (nm)	
		1:1	2:1	1:1	2:1	1:1	2:1	1:1	2:1
Malonic Acid	145	139	140	113	113	5.5	4.5	32	32
Glutaric Acid	135	133	133	106	106	1.7	1.4	28	28

809
810

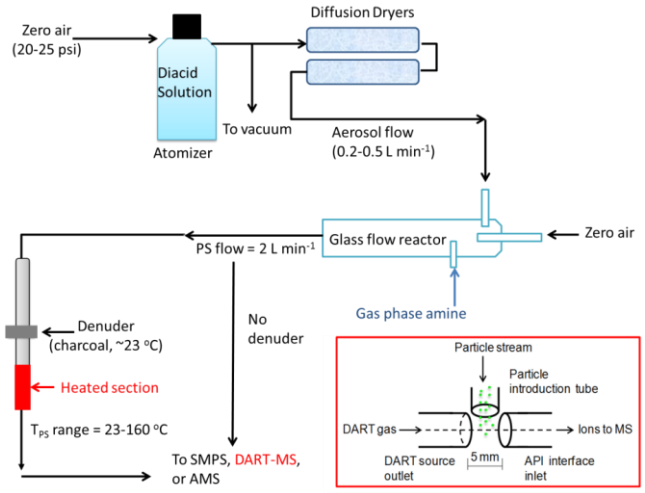

Figure 1. Schematic diagram of the experimental apparatus used for the study of the reaction of diacid particles with gas phase amines. The inset shows the configuration of DART ion source interfaced to the MS.

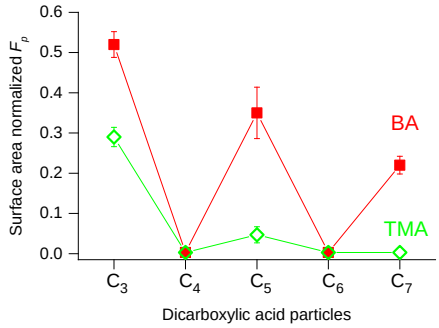

Figure 2. Surface area normalized fraction (F_p) of butylamine (solid square) and trimethylamine (open diamond) in amine-reacted C_3-C_7 dicarboxylic acid particles measured at T_{PS} = 23 °C. Error bars are ±1σ.

Comment [b12]: "fraction was added"

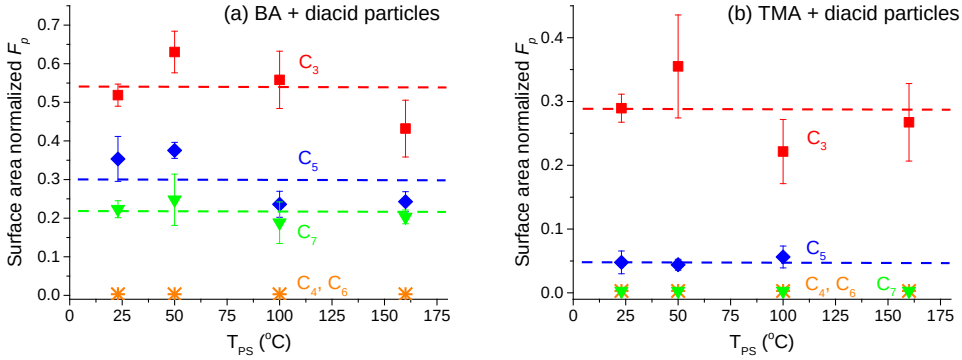

Figure 3. Surface area normalized fraction (F_p) of (a) butylamine and (b) trimethylamine in amine-reacted C_3-C_7 diacid particles measured at different particle stream heating temperatures (T_{PS}). The dashed line represents the average of F_p values at different T_{PS}. Error bars are ±1σ.

Comment [b13]: reworded for clarity

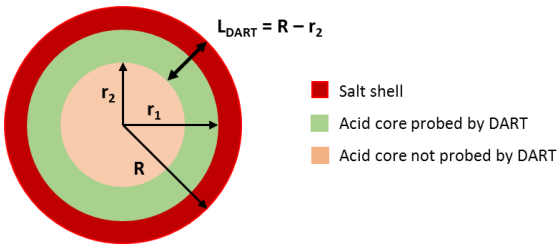

Figure 4. Schematic of a typical amine-reacted diacid particle as probed by DART-MS.

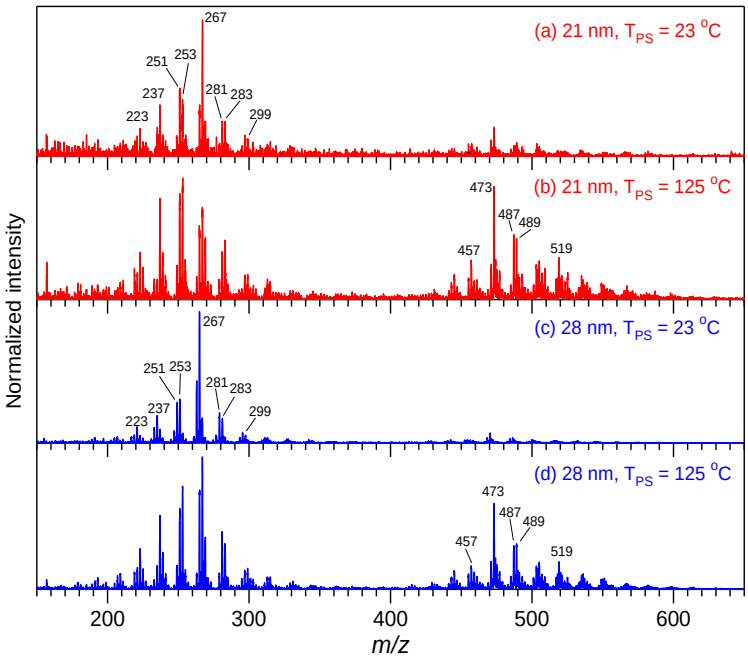

Figure 5. DART (-) mass spectra of polydisperse α-cedrene SOA particles with surface weighted geometric mean diameters ($\bar{D}_{g,S}$) of 21 nm (a, b) and 28 nm (c, d) at T_{PS} = 23 and 125 °C. T_{PS} denotes the particle stream temperature before introduction into the DART ionization region.

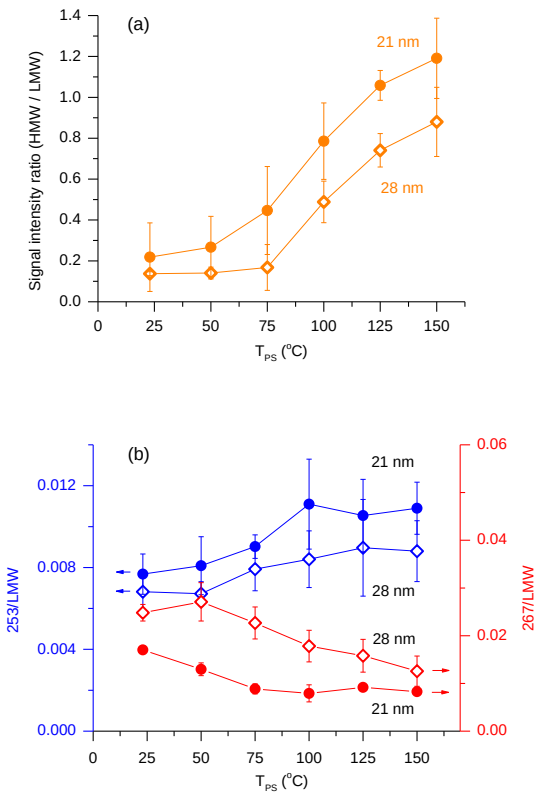

Figure 6. The DART-MS signal intensity ratio of (a) high molecular weight (HMW) products (*m/z* 420-580) to low molecular weight (LMW) products (*m/z* 200-350) and (b) products at *m/z* 253 (left y-axis) and *m/z* 267 (right y-axis) to LMW products (*m/z* 200-350) for α-cedrene SOA particles. Data represent particles with $\bar{D}_{g,S}$ of 21 nm (solid circles) and 28 nm (open diamonds) at different particle stream temperatures (T_{PS}). Error bars are ±1σ.

Supporting Information for

New insights into atmospherically relevant reaction systems using direct analysis in real time-mass spectrometry (DART-MS)

Yue Zhao, Michelle C. Fairhurst, Lisa M. Wingen, Véronique Perraud, Michael J. Ezell, and Barbara J. Finlayson-Pitts*

Department of Chemistry
University of California
Irvine, CA 92697, USA

*Corresponding author: Email: bjfinlay@uci.edu; phone: (949) 824-7670; Fax: (949) 824-2420

DART_SI_AMT Version_102716_noTrackChanges.doc

1. Particle size distributions for amine-reacted diacids and α-cedrene secondary organic aerosol (SOA) particles.

1.1 Amine-reacted diacid particles.

At the exit of the flow reactor, size distributions of the amine-reacted diacid particles were collected using a scanning mobility particle sizer (SMPS, TSI) consisting of an electrostatic classifier (model 3080), a long differential mobility analyzer (DMA, model 3081) and a condensation particle counter (model 3025A or 3776). Typical surface weighted size distributions for (a) malonic acid (C_3), (b) glutaric acid (C_5), and (c) pimelic acid (C_7) reacted particles are presented in Fig. S1, with size distribution statistics given in Table S1. To reflect the ~10% loss of amine-diacid particles in the denuder, a correction factor, C_f, of 1.1 was applied when calculating the fraction of amine in the particles, f_p.

Comment [b1]: corrected term

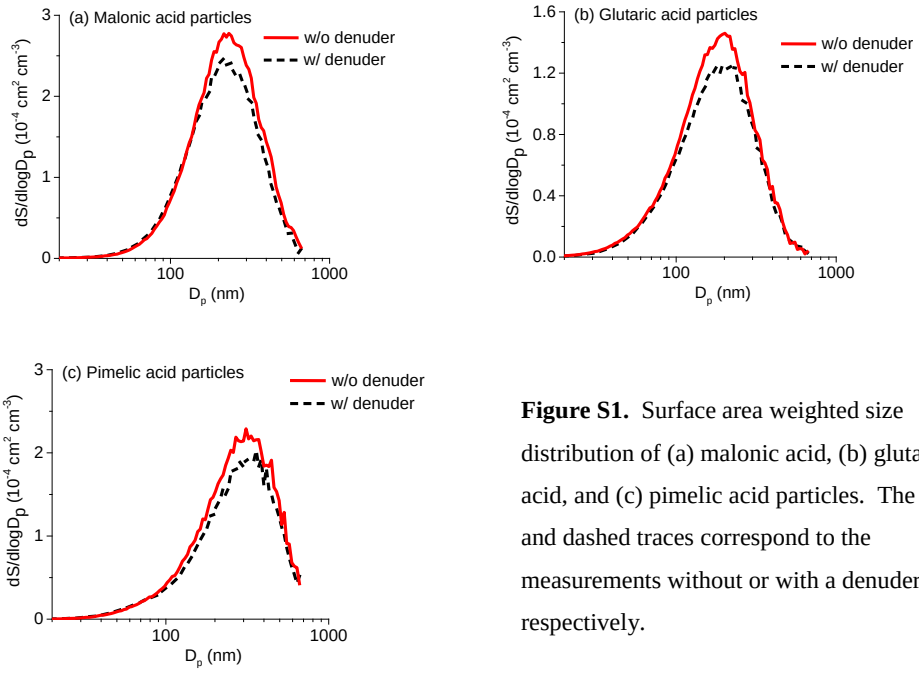

Figure S1. Surface area weighted size distribution of (a) malonic acid, (b) glutaric acid, and (c) pimelic acid particles. The solid and dashed traces correspond to the measurements without or with a denuder, respectively.

Table S1. Size Distribution Statistics for Amine-Reacted Diacid Particles[d]

	Malonic acid (C_3)	Succinic acid (C_4)	Glutaric acid (C_5)	Adipic acid (C_6)	Pimelic acid (C_7)
Surface weighted distribution:					
Total surface area (10^{-4} cm^2 cm^{-3})	1.4 ± 0.3	2.1 ± 0.1	1.1 ± 0.2	1.4 ± 0.2	1.2 ± 0.1
$\bar{D}_{g,S}$ (nm)[a]	239 ± 19	196 ± 8	211 ± 10	209 ± 9	224 ± 8
Volume weighted distribution:					
Total particle volume (10^{-10} cm^3 cm^{-3})	6.8 ± 1.4	8.1 ± 0.8	2.9 ± 0.2	5.0 ± 0.6	5.3 ± 0.5
$\bar{D}_{g,V}$ (nm)[b]	290 ± 22	258 ± 14	269 ± 13	270 ± 9	299 ± 10
Number weighted distribution:					
Total number concentration (10^5 cm^{-3})	1.7 ± 0.5	3.5 ± 0.3	1.7 ± 0.8	2.3 ± 0.2	1.8 ± 0.3
$\bar{D}_{g,N}$ (nm)[c]	103 ± 3	95 ± 2	80 ± 12	81 ± 2	86 ± 4

[a] $\bar{D}_{g,S}$: surface area weighted geometric mean diameter. [b] $\bar{D}_{g,V}$: volume weighted geometric mean diameter. [c] $\bar{D}_{g,N}$: number weighted geometric mean diameter. [d]Error bars represent ±1σ.

1.2 α-Cedrene SOA particles.

Particles exiting the flow reactor at room temperature (T_{PS} = 23°C) were measured by SMPS. A typical size distribution for α-cedrene SOA particles is presented in Fig. S2.

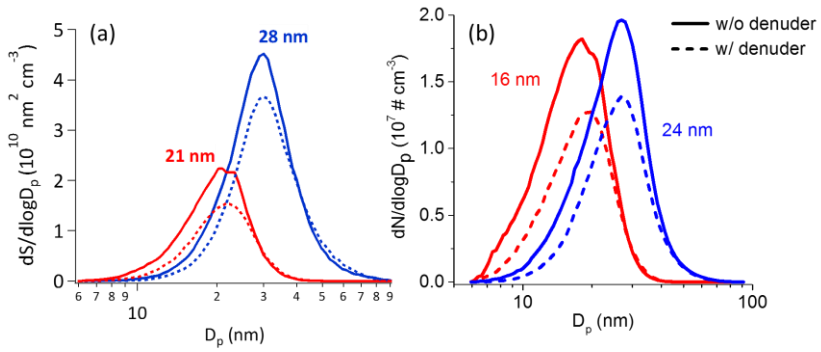

Figure S2. (a) Surface weighted size distribution of α-cedrene SOA with geometric mean diameters ($\bar{D}_{g,S}$) of 21 nm (red) and 28 nm (blue) and (b) number weighted size distribution with geometric mean diameters ($\bar{D}_{g,N}$) of 16 nm (red) and 24 nm (blue) formed in the flow reactor. The solid and dashed traces correspond to the measurements without or with a denuder, respectively at T_{PS} = 23 °C.

Comment [b2]: Reformatted the Y axis

2. Temperature in the DART ionization region

The temperature in the ionization region was measured as a function of DART gas temperature both with and without a clean air flow equivalent to that used for the particle stream by placing a thermocouple in the middle of the ionization region. Figure S3 shows that there is no significant difference of the measured temperature in the ionization region regardless of an added flow of air within the region.

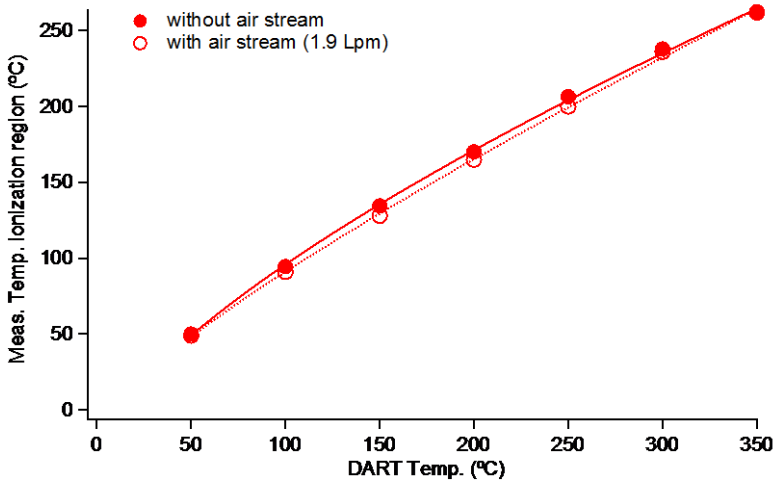

Figure S3. Measured temperature in the ionization region as a function of DART temperature with (open circles) or without (filled circles) added air flow.

3. DART mass spectra of trimethylamine (TMA)-reacted glutaric acid particles and TMA-glutaric acid aqueous standard solution

Amines were observed as their $[M+H]^+$ ions in the positive ion mode (Fig. S4a). Diacids showed fragmentation in the positive ion mode, but only the parent peak was detected in the negative ion mode (Fig. S4b). Both the amine peak in the (+) ion mode and the diacid peak in the (-) ion mode were used for quantification of amines and diacids present in reacted particles exiting the flow reactor. Protonated diacid-amine clusters were not observed either in the mass spectra for particle stream or standard solutions, but the ammonium adduct of the diacid is observed due to the ubiquitous presence of NH_3 in room air. Typical DART mass spectra are shown in Fig. S4 for glutaric acid particles reacted with TMA.

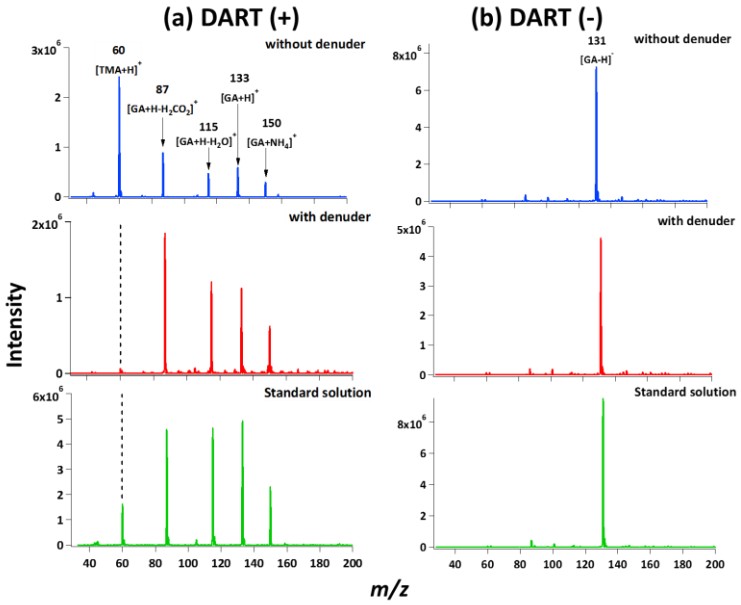

Figure S4. (a) Positive ion mode and (b) negative ion mode DART mass spectra for TMA-reacted glutaric acid (GA) particles from the flow reactor without (blue) or with (red) a denuder, and TMA-glutaric acid aqueous standard solution (green).

Comment [b3]: Changed "and" to "or" and added last part of sentence

Comment [b4]: Peak labelling was reformated and ammonium adduct added to Fig S4a

4. DART-MS calibrations for the measurement of $R_{B/A}$ values.

Standard solutions of known amine (0.5-10 mM) and diacid (10 mM) concentrations and their corresponding DART-MS intensities were used to determine the $R_{B/A}$ values for amine-reacted diacid particles based on their given intensities measured by DART-MS (see main text). All of the solutions were analyzed in the same manner and five measurements were averaged for each solution.

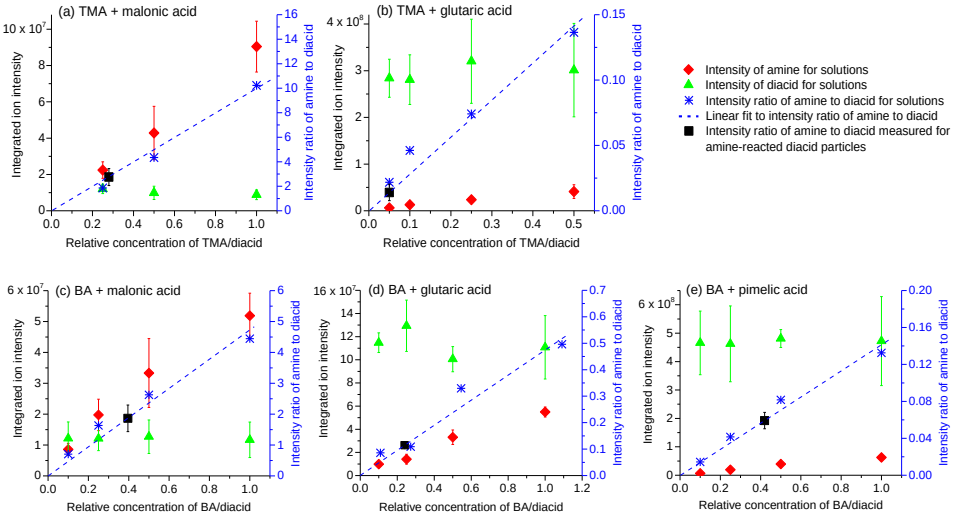

Figure S5. DART-MS signal intensity of amine (red diamond) and diacid (green triangle), as well as their intensity ratios (blue asterisk) as a function of the molar ratio of amine/diacid for different amine-diacid standard solutions. The dashed line is a linear regression fit to the intensity ratios of amine/diacid, i.e. the calibration curve. The black solid squares on each of the calibration curves represent the measured DART-MS intensity ratio of particle-bound amine to diacid, and thus determine the corresponding to the measured molar ratio of amine/diacid ($R_{B/A}$) for amine-reacted diacid particles. Error bars represent ±1σ.

5. HR-ToF-AMS measurements.

5.1 HR-ToF-AMS operating conditions and data analysis.

The chemical composition of TMA-reacted diacid particles from the flow reactor was measured using an Aerodyne high resolution time-of-flight aerosol mass spectrometer (HR-ToF-AMS). In addition, particles of ammonium nitrate and trimethylaminium chloride were sampled by atomizing from aqueous solutions of each salt using a constant output atomizer (TSI, model 3076) and two diffusion dryers (TSI, model 3062) in series. Mass spectra of these salts allowed determination of relative ionization efficiencies (RIE) of NH_4^+ and TMA. All experimental and calibration mass spectra were collected under the same AMS operating conditions: vaporizer temperature = 600 ± 2 °C, ionization energy = 70 eV; filament emission current = 1.2 mA.

5.2 Mass spectra of amine-reacted diacid particles.

Aerosol mass spectra for the amine-reacted malonic acid, glutaric acid, and pimelic acid are shown in Fig. S6. Spectra are normalized to the sum of the total peak intensity and color-coded by the families of ions observed. Fragments of the formula, $C_xH_yN_1^+$, originate from trimethylamine, while $C_xH_yO_z^+$ fragments originate from the diacids. Smaller $C_xH_y^+$ fragments may be generated from both TMA and the diacids (e.g. CH_3^+), but it is clear from Fig. S6 that there are an increasing number of $C_xH_y^+$ fragments as the carbon chain length of the diacid particles increases. The $C_xH_y^+$ fragments account for 9%, 43%, and 56% of total fragments in Fig. S6 for malonic acid, glutaric acid, and pimelic acid diacids, respectively, indicating these fragments are predominantly generated from the diacids.

The relative intensities of $C_xH_yN_1^+$ fragments decrease from malonic acid to pimelic acid indicating that the reactivity of the diacids to TMA decreases with increasing diacid chain length, in agreement with DART-MS data. The ion intensity ratio of amine to diacid present in the particles was calculated from HR-ToF-AMS spectra from the sum of amine peak intensity divided by the sum of diacid intensity for each system, each with RIE = 1. Although the relative intensity of CO_2^+ fragments to the total ion intensity can often be used to identify carboxylic acids (Aiken et al., 2007; Duplissy et al., 2011), quantification of diacids based on CO_2^+ alone for a series of diacids with increasing chain length would lead to large underestimates because of the significant intensity from $C_xH_y^+$. The use of $C_xH_y^+$ fragments to quantify the diacids is

necessary to thoroughly account for all the diacid and allow for comparisons between the systems. A more quantitative assignment of $C_xH_y^+$ fragments to TMA and each diacid is discussed in the next section.

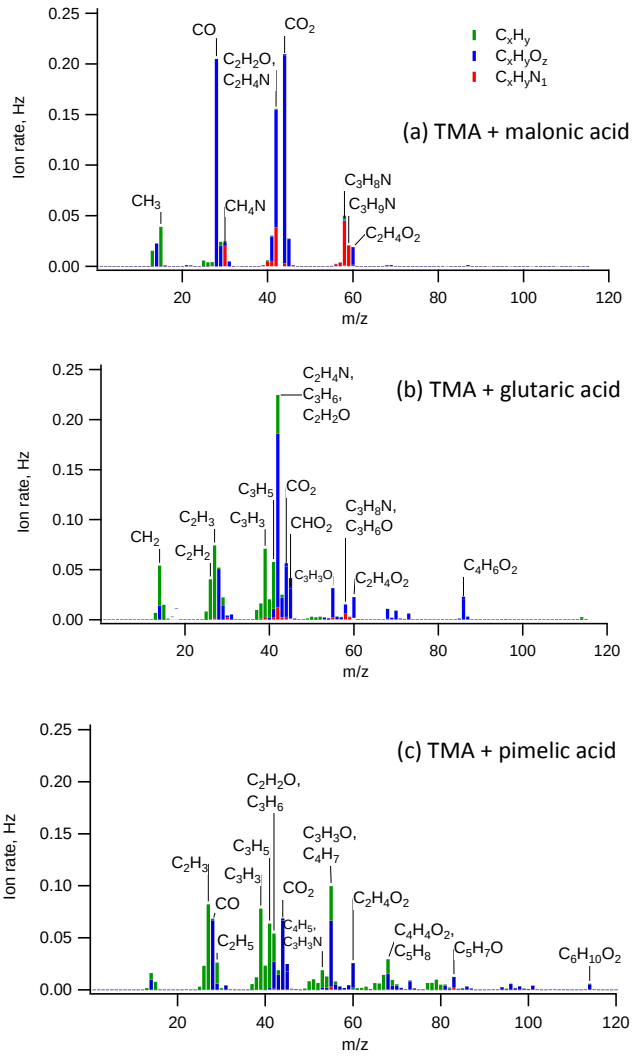

Figure S6. Aerosol mass spectra for TMA-reacted (a) malonic acid (C_3), (b) glutaric acid (C_5), and (c) pimelic acid (C_7) particles. Spectra are normalized to sum to one. Peaks are color-coded

for ion families: $C_xH_y^+$ = green, $C_xH_yO_z^+$ = blue, $C_xH_yN_1^+$ = red, and are stacked to show contributions of ion families to each nominal mass. The labels show some of the fragments that contribute to major peaks.

5.3 Calculation of molar ratios of trimethylamine to diacids.

The mass ratio may be determined from the ion intensity ratio if the RIE of each class of species is known. The accepted RIE for organics (1.4) was used to calculate the mass concentrations of the diacids (Alfarra et al., 2004; Drewnick et al., 2005). On the other hand, TMA, likely existing as an aminium ion, may be expected to have a higher RIE, similar to NH_4^+ (Canagaratna et al., 2007). Previous measurements show a wide range of 5-10 for small amines at similar AMS operating conditions (Silva et al., 2008; McGuire et al., 2014). The RIE of NH_4^+ was determined to be 3.8 ± 0.3 (1σ) through Brute Force Single Particle (BFSP) calibrations using NH_4NO_3 (Fisher, 99.9%) particles of size-selected diameters 300, 350, 400, and 450 nm. To examine the RIE for trimethylaminium ion under our specific operating conditions, particles of trimethylaminium chloride (Sigma-Aldrich, 98%) were sampled by AMS. Equation (S1) shows the relationship between the expected and observed mass intensity ratios.

$$\left(\frac{I_{TMA}}{I_{chloride}}\right)_{expected} = \left(\frac{I_{TMA}}{I_{chloride}}\right)_{observed} \cdot \frac{{}^{1}/_{RIE_{TMA}}}{{}^{1}/_{RIE_{chloride}}} \quad \text{(S1)}$$

The sum of $C_xH_yN_1^+$ fragments and minor $C_xH_y^+$ fragments was used to quantify TMA (I_{TMA}), while the sum of Cl^+ and HCl^+ fragments was used to quantify chloride ($I_{chloride}$). Mass spectra of trimethylaminium chloride are expected to give a mass ratio of amine/chloride of 1.7 (ratio of trimethylaminium (60 g mol^{-1}) to chloride (35.5 g mol^{-1})), but instead gave an observed mass ratio of 4.8. Using the default RIE for chloride (1.3) resulted in an RIE for TMA of 3.7 ± 0.1 (1σ), similar to NH_4^+.

Mass ratios of amine to diacid given by these RIE values (3.7 for TMA, 1.4 for the diacids) are then converted to molar ratios for each TMA-diacid system using the molecular weight (MW) for TMA and each diacid. Equation (S2) shows the parameters used to calculate molar ratios of amine to each diacid, $R_{B/A,AMS}$.

$$R_{B/A,AMS} = \left[\frac{\sum C_xH_yN_1^+}{\sum(C_xH_yO_z^+)+\sum(C_xH_y^+)} \cdot \frac{^1/_{RIE_{amine}}}{^1/_{RIE_{acid}}}\right] \cdot \frac{MW_{acid}}{MW_{amine}} \quad \text{(S2)}$$

The sum of $C_xH_y^+$ ions was included in the quantification of the diacid because these ions exhibit increasing ion intensity for each diacid as the carbon number of the diacid increases. However, a small contribution of $C_xH_y^+$ ions from TMA was also observed from TMA in trimethylaminium chloride mass spectra. In order to account for the contribution of $C_xH_y^+$ from TMA in trimethylaminium chloride particles, the ratios of major $C_xH_y^+$ ions to the intensity of the $C_3H_8N^+$ peak (largest amine peak) were determined from mass spectra of trimethylaminium chloride spectra. These ratios are expected to be similar in TMA-reacted diacid particle experiments. By far, the major $C_xH_y^+$ ion observed in trimethylaminium chloride spectra was CH_3^+, with a relative intensity of 0.58 to $C_3H_8N^+$. Smaller $C_xH_y^+$ peaks observed from TMA were $C_2H_3^+$ (*m/z* 27) and $C_2H_5^+$ (*m/z* 29) with relative intensities to $C_3H_8N^+$ of 0.10 and 0.11, respectively. These peaks are resolved from other ions at the same nominal mass. In TMA-reacted diacid particle mass spectra, any intensity of these $C_xH_y^+$ ions that was in excess of these ratios was attributed to the diacid.

Figure S7 shows the molar ratios determined for reaction of TMA with diacid particles with and without the correction presented above, as well as without adding any contribution from $C_xH_y^+$ for both TMA and each diacid. The correction for $C_xH_y^+$ from TMA is fairly minor, resulting in a 7% increase in the molar ratio calculated for TMA+malonic acid, 1% for TMA+glutaric acid, and 0.3% for TMA+pimelic acid. It is clear that larger $C_xH_y^+$ fragments begin to contribute significantly to the mass spectrum for glutaric acid particles and pimelic acid particles (decreasing the ratio by a factor of two for the latter). The molar ratios reported in Table 1 of the main text are those including $C_xH_y^+$ fragments with the correction discussed for TMA.

Collection efficiencies of amine-reacted diacid particles in the HR-ToF-AMS may be larger than those of the pure diacid particles, but were assumed to be equal here. Amine reactions with monocarboxylic acids in which the acid is fully titrated have been reported to create liquid particles (Lavi et al., 2015). If this is also true for amine-reacted diacid particles, it would decrease particle bounce on the HR-ToF-AMS vaporizer and increase collection efficiency relative to diacid particles that remain unreacted or less reacted. In this case, $R_{B/A}$ could be overestimated.

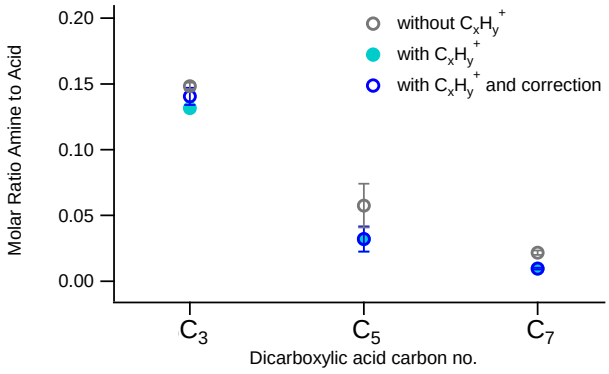

Figure S7. Molar ratio of amine to diacid observed for TMA-reacted malonic (C_3), glutaric (C_5), and pimelic (C_7) acid particles. Mass ratios (not shown) were determined by AMS using an RIE of 3.7 ± 0.1 (1σ) for TMA and the default RIE for all organics of 1.4 for each diacid and converted to molar ratios using Eq. (S2). Error bars represent 1σ of either the standard deviation of replicate measurements or the propagation of mass spectral errors and the amine RIE measurement uncertainty, whichever is greatest.

6. Estimation of the probe depth for pimelic acid particles based on their saturation vapor pressures

Chan et al. (Chan et al., 2013) used DART-MS to measure the probe depth of succinic acid (C_4), adipic acid (C_6), and suberic acid (C_8). They found that the measured probe depth is correlated with the vapor pressure (Bilde et al., 2015) of the diacids, with a measured probe depth of ~10 nm for succinic acid (P_{sat} = 7.7 × 10^{-10} atm), ~4.5 nm for adipic acid (P_{sat} = 1.9 × 10^{-10} atm), and ~1 nm for suberic acid (P_{sat} = 3.3 × 10^{-11} atm). Using the linear regression from this relationship (Fig. S8) and the vapor pressures of malonic acid, glutaric acid, and pimelic acid, respectively, probe depths for these acids were estimated. Although some uncertainty remains in the determination of the absolute probe depth using this approach, this method allows to estimate the relative probe depth between the odd acids tested in the present study. This extrapolation yields a probe depth for glutaric acid (and malonic acid) which is a factor of 8 larger than that of pimelic acid allowing for a corrected $R_{B/A}$ value of 0.05 for butylamine reacted pimelic acid particles.

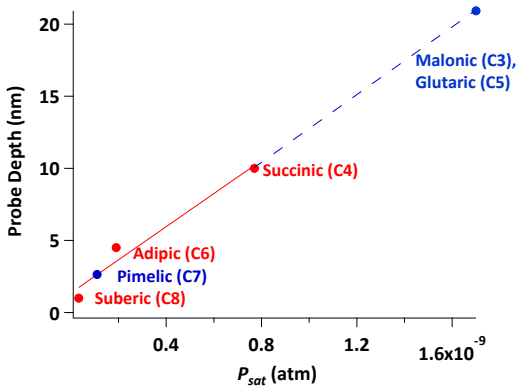

Figure S8. Linear relationship of the probe depth as a function of saturation vapor pressure (P_{sat}) for even-diacids as reported by Chan et al. (Chan et al., 2013) The red trace represents the linear regression for the even diacids: probe depth (nm) = (1.2 x 10^{10} nm/atm * P_{sat}) + 1.4.

7. Number of TMA molecules ($N_{p\text{-}amine}$) present in TMA-reacted diacid particles

Table S2. $N_{p\text{-}amine}$ values for TMA-reacted diacid systems based on DART-MS measurements.

	C_3	C_4	C_5	C_6	C_7
$N_{p\text{-}amine}$ (10^{11} molecule cm^{-3})	3.8 ± 1.1	ND	0.42 ± 0.02	ND	ND

ND: not detected. Error bars are ±1σ.

8. Evaluation of potential artifacts in DART-MS.

The ionization reactions in the DART ion source can generate reactive oxygen species such as OH and HO_2 radicals, and superoxide anion (O_2^-), along with different reagent ions (Cody et al., 2005; Gross, 2014). These species may lead to in-source oxidation of organic species, in particular for unsaturated compounds. In addition, there may be gas phase ion clustering of organic compounds in the DART ion source, which can lead to the formation of high molecular weight (HMW) species, which has been shown to occur with some ionization techniques such as ESI-MS (Gao et al., 2010; Muller et al., 2009) and CIMS with protonated water clusters or acetate as reagent ions (Aljawhary et al., 2013). In this work, these possible ionization artifacts in the DART source are evaluated to validate the interpretation of DART-MS data. Different standards including α-cedrene, C_3-C_7 diacids, hexadecanedioic acid (Sigma-Aldrich, 96%), pinonic acid (Sigma-Aldrich, 98%), and oleic acid (Sigma-Aldrich, ≥ 99%) were analyzed in the negative ion mode under DART source conditions identical to those for online particle measurements. α-Cedrene was analyzed by directly introducing its gas stream (138 ppb) into the DART ionization region. Other standards were analyzed individually by dipping a clean melting point capillary tube into their pure compounds or aqueous solutions (10 mM) and then placing it directly into the DART ionization region. In addition, the α-cedrene SOA stream, which was heated to 50 ^oC before entering into the DART ionization region, was analyzed in some experiments at a lower DART gas temperature (100 or 200 ^oC) than the temperature (350 ^oC) used for routine measurements. At these low temperatures, very low volatility HMW products in the SOA would not be effectively vaporized and the HMW ions observed in the mass spectrum,

if any, should be mainly formed by the in-source ion clustering of relatively high volatility products desorbed from SOA particles.

Figure S9a shows the DART(-) (negative ion mode) mass spectrum of 138 ppb gas phase α-cedrene. No ion signal due to α-cedrene itself corresponding to its $[M - H]^-$ (*m/z* 203) or $[M]^-$ (*m/z* 204) parent ion is observed in the mass spectra, consistent with previous studies which showed that alkenes can only be detected in the positive ion mode (Nah et al., 2013). However, strong peaks at *m/z* 235 and *m/z* 251 and relatively smaller peaks at *m/z* 237 and *m/z* 253, which are the oxidation products of α-cedrene as discussed later, are observed in the mass spectra, suggesting that oxidation of α-cedrene occurs in the DART source. Analysis of an oleic acid standard using DART-MS also showed multiple peaks corresponding to its oxidation products such as azelaic acid (from oxidative cleavage of the double bond) consistent with the detection by other techniques (Zahardis and Petrucci, 2007), OAO (one oxygen atom added to oleic acid), and OAO_2 (two oxygen atoms added) (Chan et al., 2013) with intensities of ~ 5-10% of the oleic acid parent peak. In contrast, no obvious peaks indicating oxidation chemistry were observed in DART(-) mass spectra for other standards that do not have a C=C bond. For DART-MS analysis of α-cedrene SOA particles, the particle stream was first passed through a denuder to remove the gas phase species including the unreacted α-cedrene. Additionally, since α-cedrene contains only one C=C bond, the oxidation products are unlikely to have C=C bonds. Therefore, it is expected that the DART-MS analysis presented below would not suffer from an in-source oxidation artifact.

Figures S9b and S9c show the DART(-) mass spectra of α-cedrene SOA particles where the particle stream was heated to T_{PS} = 50 ^{o}C and the DART gas temperature (T_{DART}) was either 100 or 200 ^{o}C. Only low molecular weight (LMW) ions are observed in the mass spectra, as expected if the HMW products in the SOA particles were not effectively vaporized under these analysis conditions. The absence of HMW ions in the mass spectra also suggests that the in-source clustering of components of α-cedrene SOA particles is not important. The DART(-) mass spectra of standard compounds also show negligible contributions from HMW ions except for malonic acid, for which the acid dimer is observed with its intensity being ~ 20% of that of the monomer.

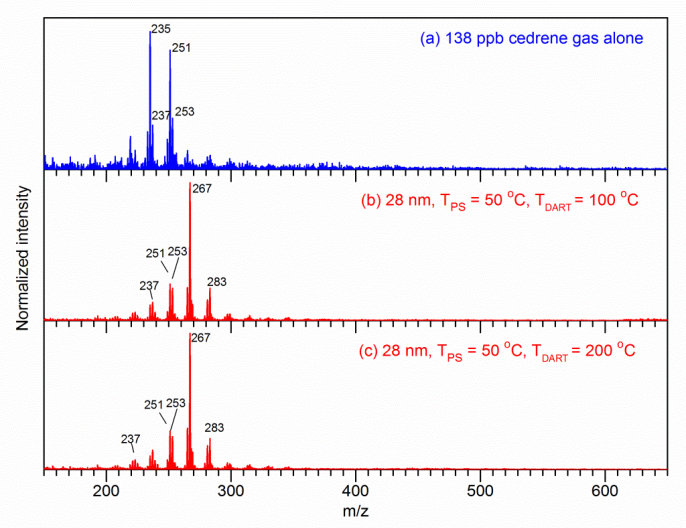

281

282 **Figure S9.** DART(-) mass spectra of (a) α-cedrene gas, (b) α-cedrene SOA particles at T_{DART} =

283 100 °C, and (c) α-cedrene SOA particles at T_{DART} = 200 °C. T_{PS} denotes the particle stream

284 heating temperature before introduction into the ionization region, which is 50 °C for (b) and (c).

285 T_{DART} represents the DART gas temperature.

286

References:

Aiken, A. C., DeCarlo, P. F., and Jimenez, J. L.: Elemental analysis of organic species with electron ionization high-resolution mass spectrometry, Anal. Chem., 79, 8350-8358, 2007.

Alfarra, M. R., Coe, H., Allan, J. D., Bower, K. N., Boudries, H., Canagaratna, M. R., Jimenez, J. L., Jayne, J. T., Garforth, A. A., and Li, S.-M.: Characterization of urban and rural organic particulate in the Lower Fraser Valley using two Aerodyne aerosol mass spectrometers, Atmos. Environ., 38, 5745-5758, 2004.

Aljawhary, D., Lee, A. K. Y., and Abbatt, J. P. D.: High-resolution chemical ionization mass spectrometry (ToF-CIMS): application to study SOA composition and processing, Atmos. Meas. Tech., 6, 3211-3224, 2013.

Bilde, M., Barsanti, K., Booth, M., Cappa, C. D., Donahue, N. M., Emanuelsson, E. U., McFiggans, G., Krieger, U. K., Marcolli, C., Tropping, D., Ziemann, P., Barley, M., Clegg, S., Dennis-Smither, B., Hallquist, M., Hallquist, A. M., Khlystov, A., Kulmala, M., Mogensen, D., Percival, C. J., Pope, F., Reid, J. P., da Silva, M. A. V. R., Rosenoern, T., Salo, K., Soonsin, V. P., Yli-Juuti, T., Prisle, N. L., Pagels, J., Rarey, J., Zardini, A. A., and Riipinen, I.: Saturation vapor pressures and transition enthalpies of low-volatility organic molecules of atmospheric relevance: from dicarboxylic acids to complex mixtures, Chem. Rev., 115, 4115-4156, 2015.

Canagaratna, M., Jayne, J., Jimenez, J., Allan, J., Alfarra, M., Zhang, Q., Onasch, T., Drewnick, F., Coe, H., and Middlebrook, A.: Chemical and microphysical characterization of ambient aerosols with the Aerodyne aerosol mass spectrometer, Mass Spectrom. Rev., 26, 185-222, 2007.

Chan, M. N., Nah, T., and Wilson, K. R.: Real time *in situ* chemical characterization of sub-micron organic aerosols using direct analysis in real time mass spectrometry (DART-MS): the effect of aerosol size and volatility, Analyst, 138, 3749-3757, 2013.

Cody, R. B., Laramee, J. A., and Durst, H. D.: Versatile new ion source for the analysis of materials in open air under ambient conditions, Anal. Chem., 77, 2297-2302, 2005.

Drewnick, F., Hings, S. S., DeCarlo, P., Jayne, J. T., Gonin, M., Fuhrer, K., Weimer, S., Jimenez, J. L., Demerjian, K. L., and Borrmann, S.: A new time-of-flight aerosol mass spectrometer (TOF-AMS)—instrument description and first field deployment, Aerosol Sci. Tech., 39, 637-658, 2005.

Duplissy, J., DeCarlo, P. F., Dommen, J., Alfarra, M. R., Metzger, A., Barmpadimos, I., Prevot, A. S., Weingartner, E., Tritscher, T., and Gysel, M.: Relating hygroscopicity and composition of organic aerosol particulate matter, Atmos. Chem. Phys., 11, 1155-1165, 2011.

Gao, Y. Q., Hall, W. A., and Johnston, M. V.: Molecular composition of monoterpene secondary organic aerosol at low mass loading, Environ. Sci. Technol., 44, 7897-7902, 2010.

Gross, J. H.: Direct analysis in real time-a critical review on DART-MS, Anal. Bioanal. Chem., 406, 63-80, 2014.

Lavi, A., Segre, E., Gomez-Hernandez, M., Zhang, R. Y., and Rudich, Y.: Volatility of atmospherically relevant alkylaminium carboxylate salts, J. Phys. Chem. A, 119, 4336-4346, 2015.

McGuire, M. L., Chang, R. Y. W., Slowik, J. G., Jeong, C. H., Healy, R. M., Lu, G., Mihele, C., Abbatt, J. P. D., Brook, J. R., and Evans, G. J.: Enhancing non-refractory aerosol apportionment from an urban industrial site through receptor modeling of complete high time-resolution aerosol mass spectra, Atmos. Chem. Phys., 14, 8017-8042, 2014.

Muller, L., Reinnig, M. C., Hayen, H., and Hoffmann, T.: Characterization of oligomeric compounds in secondary organic aerosol using liquid chromatography coupled to electrospray ionization Fourier transform ion cyclotron resonance mass spectrometry, Rapid Commun. Mass Spectrom., 23, 971-979, 2009.

Nah, T., Chan, M., Leone, S. R., and Wilson, K. R.: Real time *in situ* chemical characterization of submicrometer organic particles using direct analysis in real time-mass spectrometry, Anal. Chem., 85, 2087-2095, 2013.

Silva, P. J., Erupe, M. E., Price, D., Elias, J., GJ Malloy, Q., Li, Q., Warren, B., and Cocker III, D. R.: Trimethylamine as precursor to secondary organic aerosol formation via nitrate radical reaction in the atmosphere, Environ. Sci. Technol., 42, 4689-4696, 2008.

Zahardis, J., and Petrucci, G. A.: The oleic acid-ozone heterogeneous reaction system: products, kinetics, secondary chemistry, and atmospheric implications of a model system - a review, Atmos. Chem. Phys., 7, 1237-1274, 2007.